Immunobiology 217 (2012) 281–297

Contents lists available at SciVerse ScienceDirect

Immunobiology

journal homepage: www.elsevier.de/imbio

Review

Complement Factor H–ligand interactions: Self-association, multivalency and dissociation constants

Stephen J. Perkins*, Ruodan Nan, Keying Li, Sanaullah Khan, Ami Miller

Department of Structural and Molecular Biology, Darwin Building, University College London, Gower Street, London WC1E 6BT, UK

ARTICLE INFO

Article history:
Received 19 July 2011
Received in revised form 7 October 2011
Accepted 13 October 2011

Keywords:
Analytical ultracentrifugation
Surface plasmon resonance
X-ray scattering
Complement Factor H
Complement C3

ABSTRACT

Factor H (FH) is the major plasma regulator of the central complement protein C3b in the alternative pathway of complement activation. The elucidation of the FH interactions with five major ligands (below) is complicated by their weak μM dissociation constants K_D and FH multivalency. We present the first survey of all the K_D values for the major FH–ligand interactions and critically review their physiological significance.

(i) FH self-association is presently well-established. We review multiple data sets that show that 5–14% of FH is self-associated in physiological conditions. FH self-association is significant for both laboratory investigations and physiological function.
(ii) The FH–C3b complex shows low μM affinity, meaning that the complex is not fully formed in plasma. In addition, C3, its hydrolysed form C3u, and its cleaved forms C3b and C3d show multimerisation. Current data favour a model when two C3b molecules bind independently to one FH molecule, as opposed to a 1:1 stoichiometry where FH wraps itself around C3b.
(iii) Heparin is often used as an analogue of the polyanionic host cell surface. The FH–heparin complex also shows a low μM affinity, again meaning that complexes are not fully formed *in vivo*. The oligomeric FH–heparin complexes clarify a two-site interaction model of FH with host-cell surfaces.
(iv) Reinvestigation of the FH and C-reactive protein (CRP) interaction revealed that this can only occur in plasma when CRP levels are elevated during acute-phase conditions. Given that CRP binds more weakly to the His402 allotype of FH than the Tyr402 allotype, this suggested a link with age-related macular degeneration (AMD).
(v) FH activity is inhibited by zinc, which causes FH to aggregate strongly. High levels of bioavailable zinc occur in sub-retinal pigment epithelial deposits which lead to AMD. Excess zinc binds weakly to a central region of FH, explaining how zinc inhibits FH regulation of C3b.

Contents

Abbreviations: AMD, age-related macular degeneration; aHUS, atypical haemolytic uraemic syndrome; K_D, dissociation constant; CRP, C-reactive protein; FH, Factor H; SCR, short complement regulator.

* Corresponding author. Tel.: +44 20 7679 7048; fax: +44 20 7679 7193.
E-mail address: s.perkins@ucl.ac.uk (S.J. Perkins).

0171-2985/$ – see front matter © 2011 Elsevier GmbH. All rights reserved.
doi:10.1016/j.imbio.2011.10.003

Complement Factor H interactions in plasma

In plasma, the serum proteins total about 70 mg/ml. The most overwhelmingly abundant protein (60% of the total) is human serum albumin (molecular weight 65,000 Da) that circulates in plasma at reference levels between 30 and 50 mg/ml (450–750 μM) (Putnam 1975; Lu et al. 2008). This is followed by the immunoglobulins (10–15 mg/ml; IgG molecular weight 150 kDa; concentration 67–100 μM). Five plasma proteins present in moderate amounts include fibrinogen (2–5 mg/ml; 169 kDa; 9 μM), α_1-antitrypsin (2–4 mg/ml; 40 kDa), haptoglobulin (1–2.2 mg/ml; 100 kDa), α_2-macroglobulin (1.5–4.2 mg/ml; 725 kDa), and transferrin (2–4 mg/ml; 77 kDa) (Putnam 1975). The 30–40 complement proteins (Walport 2001; Janeway et al. 2005) make up 2.6 mg/ml in total, and many are typically present at concentrations in the 0.3–7 μM range (Law and Reid 1995). The plasma concentrations of acute phase proteins increase or decrease in response to inflammation. Under acute phase conditions, some complement protein concentrations and related ones, including C3, C4 and especially C-reactive protein (CRP), go much higher. Many of the complement proteins are therefore abundant in comparison to other serum proteins such as the coagulation cascade proteases. The six coagulation Factors V, VII, VIII, IX, X and XI, together with von Willebrand factor, circulate at 0.1–10 μg/ml which corresponds to nanomolar levels of protein (0.3–135 nM). Modern proteomics methods complete the picture by showing that there are as many as 1000–2000 other plasma proteins with concentrations reaching as low as picomolar levels (5 ng/ml) (Anderson 2010).

Complement is a major defence and clearance system in blood, this being activated by pathogens such as bacteria by one of three pathways, the classical, lectin or alternative pathways. All three pathways lead to the activation of C3, the central complement component, to C3b (Fig. 1). C3b formation ultimately leads to the formation of a membrane attack complex that lyses bacteria and the clearance of C3b-opsonized cells by phagocytosis. The C3b level requires regulation. Too much C3b activation will lead to host damage, while too little C3b activation means that the host becomes susceptible to infection. This is often referred to as the "double-edged sword" nature of complement activation and regulation (Zipfel and Skerka 2009; Ricklin et al. 2010). In the context of the plasma proteins, both C3 and the major C3b regulator Factor H (FH: Fig. 1) are comparatively abundant. C3 is reported in typical concentration ranges of 1.0 mg/ml, 1.3 mg/ml or 1.6 mg/ml (5–8.5 μM) (Putnam 1975; Law and Reid1995; Nilsson and Ekdahl 1998), while FH is reported to be at 0.116–0.562 mg/ml (0.8–3.6 μM) (Rodriguez de Cordoba and Goicoechea de Jorge 2008) and 0.235–0.81 mg/ml (2–5 μM) (Saunders et al. 2006). C3 exhibits a modest acute-phase response with a 50% increase in plasma concentration (Gabay and Kushner 2001). The comparative abundance of C3 is most likely to result from an essential requirement to maintain enough C3 in plasma in order to combat infections, while the abundance of FH is attributable to the need to adequately regulate C3b for host protection. This C3b regulation is achieved by the two-fold role of FH in (i) blocking the binding of complement Factor B to C3b, and competing with and displacing the Bb fragment that binds to C3b to form the C3b convertase enzyme that generates even more C3b, and (ii) acting as a cofactor of the protease Factor I for the proteolytic cleavage of C3b to form the inactive fragments C3d and C3c. FH functions both in solution in plasma and also by binding to host cell surfaces through interactions with oligosaccharides bearing clusters of negative charges or motifs of high negative charge density.

The strength of the FH–C3b interaction and others is key to understanding this crucial stage of complement activation. This is monitored by the dissociation constant K_D. The K_D value for an interaction is also often comparable to the macromolecular concentrations. Given that C3 and FH are found at 2–7 μM levels in plasma, it is unsurprising that the K_D values for their ligand interactions are also in similar μM ranges. In this review, the FH and ligand concentrations are accordingly reported in both mg/ml and μM units. For a 1:1 FH–ligand equilibrium, the K_D value is given by [FH][ligand]/[complex], and K_D corresponds to the FH concentration at which the complex is 50% dissociated. It is noteworthy that the absence of strong FH affinities with K_D values in nM ranges means that FH participates only in partially formed complexes with C3b and heparin. The μM affinities for FH–ligand complexes mean that these moderately strong interactions can be missed in biochemical assays. Examples of this will be noted below in relation to FH–CRP and FH–zinc interaction studies.

In addition to the weak μM K_D values, an understanding of FH–ligand interactions is also complicated for two additional reasons. Firstly, FH undergoes 5–14% self-association, both in the test-tube and in physiological milieu (Nan et al. 2008a). This is disregarded by some investigators; their resulting analyses of FH interactions do not take advantage of this knowledge and the conclusions can be misleading. Examples will be noted below in relation to studies of FH itself, and in the FH–C3b and FH–heparin interaction studies. Secondly, FH undergoes multivalent interactions with its C3b, C3d, heparin and CRP ligands. Multivalency means that the conventional analyses of protein complexes in terms of simple 1:1 interactions may not be adequate in quantitative studies. In particular for FH, the study of small recombinant FH fragments–ligand complexes requires comparisons with the interaction based on full-length FH as a control. An example discussed later involves the interaction between C3d and FH.

Many FH–ligand interactions are formed through opposing ionic interactions between FH and its ligands. Given the weak μM K_D values, the interactions become stronger and more easily observed if buffer compositions with reduced salt levels such as 50 mM NaCl are used in place of the plasma level of 137 mM NaCl and 11 mM phosphate. Higher salt levels than those in plasma will inhibit interactions that have an electrostatic component. Comparisons with low (50 mM NaCl) and high (250 mM NaCl) salt levels are useful to unravel the significance of electrostatic forces for a given FH–ligand interaction. However the use of 50 mM NaCl buffer can promote non-physiological interactions between FH and its ligands. An example of this involves C3d self-association (Table 1). Low salt was used in many of the first studies of the FH interactions with its ligands, and the K_D values are reduced (stronger binding) for this reason (Table 1). An example is discussed in more detail for the FH–CRP interaction.

The use of 137 mM NaCl is preferred for FH–ligand studies, while 150 mM NaCl is also reasonable. Blood pH is regulated to stay within the narrow range of 7.35–7.45, and this pH is principally determined by the bicarbonate equilibrium and the surface histidine residues of haemoglobin. In that context, blood contains phosphate (a ratio of 1:4 NaH_2PO_4 and Na_2HPO_4 yields a pH of 7.4). Dulbecco's Phosphate Buffered Saline (PBS) is a standard buffer used to replicate plasma buffer, with a formulation of 137 mM NaCl, 2.7 mM KCl, 8.1 mM Na_2HPO_4, 1.76 mM KH_2PO_4, pH 7.4 (Dulbecco

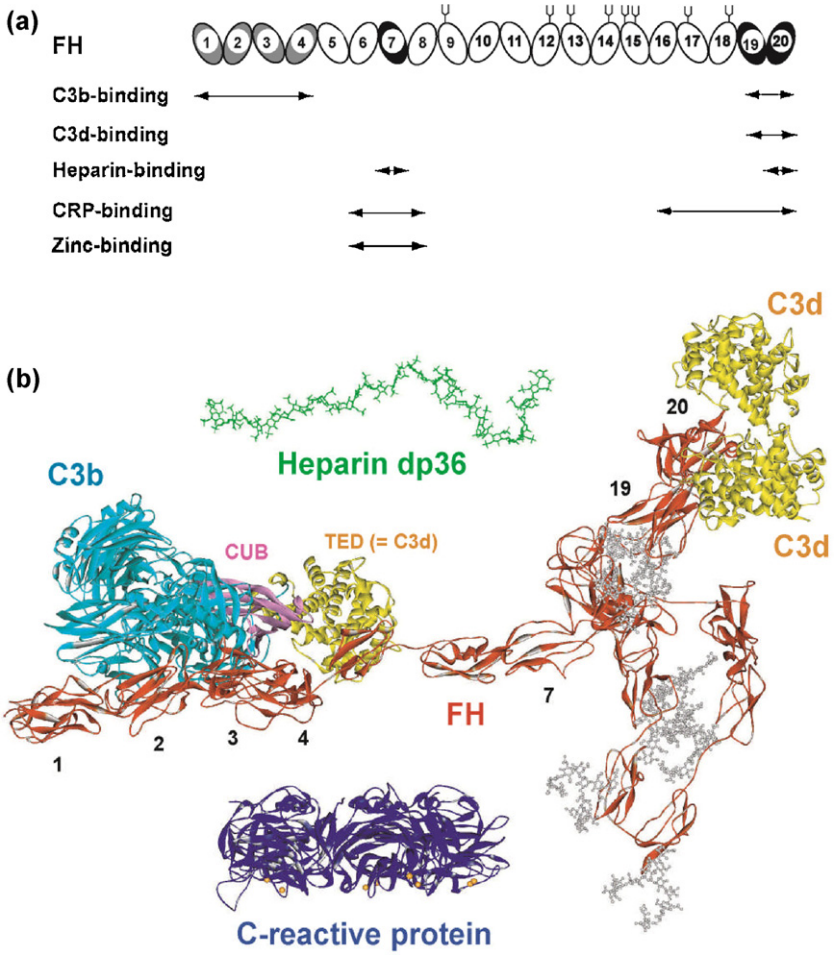

Fig. 1. Domain structure of Factor H and its ligands. (a) Schematic view of the 20 SCR domains of FH. The positions of two C3b binding sites (SCR-1/4 having decay accelerating and factor I activity), two heparin-binding sites on SCR-7 and SCR-20, two C3d binding sites on SCR-19 and SCR-20, two C-reactive protein binding sites at SCR-6/8 and SCR-16/20, and weak zinc binding sites at SCR-6/8 are shown schematically. The location of eight N-linked glycosylation sites is shown by symbols; a ninth site at SCR-4 is not occupied. (b) Comparison of molecular views to the same scale of a solution structure for FH with structures for its C3b, C3d, heparin and CRP ligands. A folded-back domain arrangement of a best-fit FH structural model is shown with its longest length running from left to right (SCR-1 to SCR-20). The FH structure is from two recent studies (Okemefuna et al. 2009a; Nan et al. 2010). The C3b-binding SCR-1/4 domains are shown in red, with C3b shown in cyan, and its CUB and TED domains shown in purple and yellow. The heparin- and CRP-binding SCR-7 domain is shown in red, with the CRP pentamer shown edge-on in blue. The bent SCR central region of FH with the shorter and glycosylated SCR domains are shown to the bottom right. The two C3d proteins bound to SCR-19 and SCR-20 are shown in yellow, while heparin dp36 (18 disaccharides; dp stands for degree of polymerisation) is shown in green. The eight FH oligosaccharides are shown in grey. (For interpretation of the references to color in this figure legend, the reader is referred to the web version of the article.)

and Vogt 1954). PBS has many uses because it is isotonic and non-toxic to cells. Its osmolarity and ion concentration matches that of the human body. If required, such as in studies with CRP, 2 mM calcium should be added to correspond to the 2.5 mM level of calcium found in plasma (Hurwitz 1996). Normal saline used in intravenous drips contains 154 mM NaCl, which is slightly higher in osmolarity than that found in blood. This higher NaCl level compensates for the presence of 11 mM phosphate in PBS, i.e. the presence of other proteins and chemicals in plasma. Twelve buffering agents have been described that are good candidates for biological work (Good et al. 1966). These include HEPES (pK 7.55) which is advantageous when zinc is present so long as 137 mM NaCl is also present (Table 1), because phosphate is precipitated by zinc.

Here, we review FH in terms of FH, C3 and CRP self-association, FH multivalency, and a survey of all the known dissociation constants K_D for its FH–ligand interactions. These are discussed in the context of FH and ligand concentrations and the experimental buffers in use. Other recent reviews of FH interactions discuss FH in relation to age-related macular degeneration (AMD) (Perkins et al. 2010a) and the biophysical basis of the FH–CRP interaction (Perkins et al. 2010b). The functional context of FH in diseases such as AMD and atypical haemolytic uraemic syndrome (aHUS) is reviewed elsewhere (Rodriguez de Cordoba and Goicoechea de Jorge 2008; Holers 2008; Zipfel and Skerka 2009; Ricklin et al. 2010). For example, the Tyr402His polymorphism in FH enhances the risk for AMD.

Interaction sites of Factor H by biophysical methods

In summary, FH is constructed from 20 short complement regulator (SCR) domains, each of length about 61 residues, joined by linkers between 3 and 8 residues in size (Fig. 1). The SCR domains constitute the most abundant domain type in the complement system. They were originally termed as “short consensus repeat” (SCR) and subsequently as “complement control protein” (CCP) domains. The redefinition of SCR as “short complement regulator” makes better sense of this more commonly used acronym. FH has major N-terminal and C-terminal binding sites for C3b at SCR-1/4 and SCR-19/20 (Fig. 1a) (Schmidt et al. 2008). A third C3b binding site specific for C3c has been proposed in the central part of FH (Sharma and Pangburn 1996; Jokiranta et al. 2000; Schmidt et al. 2008). There are also two heparin binding sites at SCR-7/8 and SCR-19/20

Table 1
Survey of dissociation constants K_D for the FH interactions with its ligands.

Interaction	K_D (μM)	Method[a]	Buffer (abbreviated)	Reference
FH self-association				
FH–FH	28	SE	10 mM HEPES with 137 mM NaCl and EDTA, pH 7.4	Nan et al. (2008a)
FH–FH	>8	SPR	10 mM HEPES with 137 mM NaCl and EDTA, pH 7.4	Nan et al. (2010)
SCR-6/8–SCR-6/8 (His402)	40	SE	PBS with 137 mM NaCl, pH 7.3	Fernando et al. (2007)
SCR-16/20–SCR-16/20	13–18	SE, SAXS	PBS with 137 mM NaCl, pH 7.3	Okemefuna et al. (2008)
FH–C3 interactions				
C3d–C3d	23	SE	10 mM HEPES, 50 mM NaCl, pH 7.4	Perkins et al. (2005, 2008)
C3d–C3d	No complex	SV	PBS with 137 mM NaCl, pH 7.4	Li et al. (2008)
C3–C3; C3u–C3u	38	SV	PBS with 50 mM NaCl, pH 7.4	Li et al. (2010)
C3–C3; C3u–C3u	38–53	SV	PBS with 137 mM NaCl, pH 7.4	Li et al. (2010)
FH–C3b	0.59–1.6	SPR	10 mM HEPES with 150 mM NaCl, EDTA and surfactant, pH 7.4	Schmidt et al. (2008)
rFH and FH–C3b	1.5–2.9	SPR	10 mM HEPES with 150 mM NaCl, Mg and surfactant, pH 7.4	Schmidt et al. (2011)
FH–C3u	0.11	SV	PBS with 50 mM NaCl, pH 7.4	Li (2010)
FH–C3u	0.59	SV	PBS with 137 mM NaCl, pH 7.4	Li (2010)
SCR-1/4–C3b	11	SPR	PBS with 150 mM NaCl and surfactant, pH 7.4	Wu et al. (2009)
SCR-1/4–C3b	9.8–13.5	SPR	10 mM HEPES with 150 mM NaCl, EDTA and surfactant, pH 7.4	Schmidt et al. (2008)
SCR-19/20–C3b	5.4	SPR	PBS with 140 mM NaCl, pH 7.3	Jokiranta et al. (2006)
SCR-19/20–C3b	3.5–4.5	SPR	10 mM HEPES with 150 mM NaCl, EDTA and surfactant, pH 7.4	Schmidt et al. (2008)
SCR-19/20–C3b	0.54	SPR	10 mM HEPES with 150 mM NaCl, EDTA and surfactant, pH 7.2	Kajander et al. (2011)
SCR-15/20–C3d	0.088	SPR	Veronal with 75 mM NaCl, pH 7.4	Hellwage et al. (2002)
SCR-16/20–C3d	1.0	SPR	10 mM HEPES with 50 mM NaCl, pH 7.4	Okemefuna et al. (2009a,b)
SCR-16/20–C3d	2.6	SPR	10 mM HEPES with 137 mM NaCl, pH 7.4	Okemefuna et al. (2009a,b)
SCR-19/20–C3d	0.18	SPR	10 mM HEPES with 150 mM NaCl, EDTA and surfactant, pH 7.2	Kajander et al. (2011)
SCR-19/20–C3d	6.2–8.2	SPR	10 mM HEPES with 150 mM NaCl, Mg and surfactant, pH 7.4	Morgan et al. (2011)
FH–heparin interactions				
FH–commercial heparin	0.0092	SPR	PBS with 50 mM phosphate, 100 mM NaCl, pH 7.2	Yu et al. (2007)
SCR-19/20–heparin dp4	9.0	NMR	20 mM acetate with 200 mM NaCl, pH 4.0	Herbert et al. (2006)
SCR-6/8 (His402)–heparin dp10	<14[b]	SV	PBS with 137 mM NaCl, pH 7.3	Fernando et al. (2007)
FH–heparin dp30/dp36	~0.5	SV	10 mM HEPES with 137 mM NaCl, pH 7.4	Khan (2011)
FH–CRP interactions				
CRP–Ca	60	ED	50 mM Tris, 100 mM NaCl, pH 7.5	Kinoshita et al. (1989)
CRP–Ca	30	SPR	10 mM HEPES, 100 mM NaCl, pH 7.4	Christopeit et al. (2009)
CRP–CRP	19	SV	10 mM Tris, 50 mM NaCl, 2 mM $CaCl_2$, pH 8.0	Okemefuna et al. (2010a)
CRP–CRP	16–26	SPR, SAXS	10 mM Tris, 140 mM NaCl, 2 mM $CaCl_2$, pH 8.0	Okemefuna et al. (2010a)
FH–CRP	4.2	SPR	10 mM Tris, 137 mM NaCl, 2 mM $CaCl_2$, pH 7.4	Okemefuna et al. (2010b)
SCR-6/8 (Tyr402)–CRP	3.9	SPR	10 mM HEPES, 137 mM NaCl, 2 mM $CaCl_2$, pH 7.4	Okemefuna et al. (2010b)
SCR-6/8 (His402)–CRP	11.9	SPR	10 mM HEPES, 137 mM NaCl, 2 mM $CaCl_2$, pH 7.4	Okemefuna et al. (2010b)
SCR-16/20–CRP	15.3	SPR	10 mM HEPES, 137 mM NaCl, 2 mM $CaCl_2$, pH 7.4	Okemefuna et al. (2010b)
FH–zinc interactions				
FH–zinc	~10[b]	SAXS	10 mM HEPES, 137 mM NaCl, pH 7.4	Nan et al. (2008b, 2011)
SCR-6/8–zinc	~10[b]	SAXS	10 mM HEPES, 137 mM NaCl, pH 7.4	Nan et al. (2011)

[a] ED, equilibrium dialysis; SAXS, small-angle X-ray scattering; SE, sedimentation equilibrium; SPR, surface plasmon resonance; SV, sedimentation velocity.
[b] The K_D value was estimated from the protein or ligand concentrations in use.

of FH (Schmidt et al. 2008). There are CRP binding sites within SCR-6/8 and SCR-16/20 of FH (Okemefuna et al. 2010b). Weak zinc binding sites are mostly located within SCR-6/8 (Nan et al. 2011). The absence of a high resolution crystal structure for FH is attributable to its large size, glycosylation and presumed inter-SCR flexibility. To compensate for this, folded-back solution structures for intact FH at medium structural resolution were determined by a combination of X-ray scattering, analytical ultracentrifugation and molecular modelling (Aslam and Perkins 2001; Okemefuna et al. 2009a). At present, a total of 14 high resolution SCR structures of the 20 are known, using crystallography for SCR-1/4, SCR-6/8, and SCR-19/20 (Jokiranta et al. 2006; Prosser et al. 2007; Wu et al. 2009; Kajander et al. 2011; Morgan et al. 2011), and NMR for SCR-1/3, SCR-5, SCR-7, SCR-12/13, SCR-15/16 and SCR-19/20 (Hocking et al. 2008; Schmidt et al. 2010). Eleven of these structures have been incorporated in the latest full length FH model, which has been updated further (Fig. 1b) (Okemefuna et al. 2009a; Nan et al. 2010).

Biophysical methods for looking at the quantitative FH interactions with itself and with four ligands include analytical ultracentrifugation, X-ray scattering and surface plasmon resonance. The K_D values of the interactions can be obtained from all three methods. In addition, structural information can also be obtained from ultracentrifugation and scattering. The velocity method in ultracentrifugation involves sample sedimentation at high rotor speeds, and analyses of the boundaries measured with time lead to the size distribution function $c(s)$. Ultracentrifugation is more powerful than the other two methods because the presence of multiple species in the sample is revealed by separate peaks with their sedimentation coefficients $s_{20,w}$ in the $c(s)$ analyses (after correction to 20 °C and the density of water). The K_D values are obtained from integration of these individual $c(s)$ peaks (Okemefuna et al. 2010a). The classic sedimentation equilibrium approach also leads to K_D values by the fits of sedimentation curves recorded at equilibrium for different concentrations and rotor speeds (Nan et al. 2008a). Scattering measures the diffraction from protein solutions. If scattering is used for determining K_D values, the scattering curves need to be known for the unbound structures as well as for the complex (Okemefuna et al. 2010a,b). From these, the ratio of the unbound and complexed species can be determined by fits of scattering curves measured in a concentration range. Surface plasmon resonance is used to study the on-rate and off-rate of a soluble "analyte" flowed over and binding to an immobilised interaction partner (the "ligand"). If these rates are slow enough, the ratio of the off-rate/on-rate gives the K_D value. If these rates are rapid, the response unit values of the bound analyte measured as a function of its concentration given an association curve

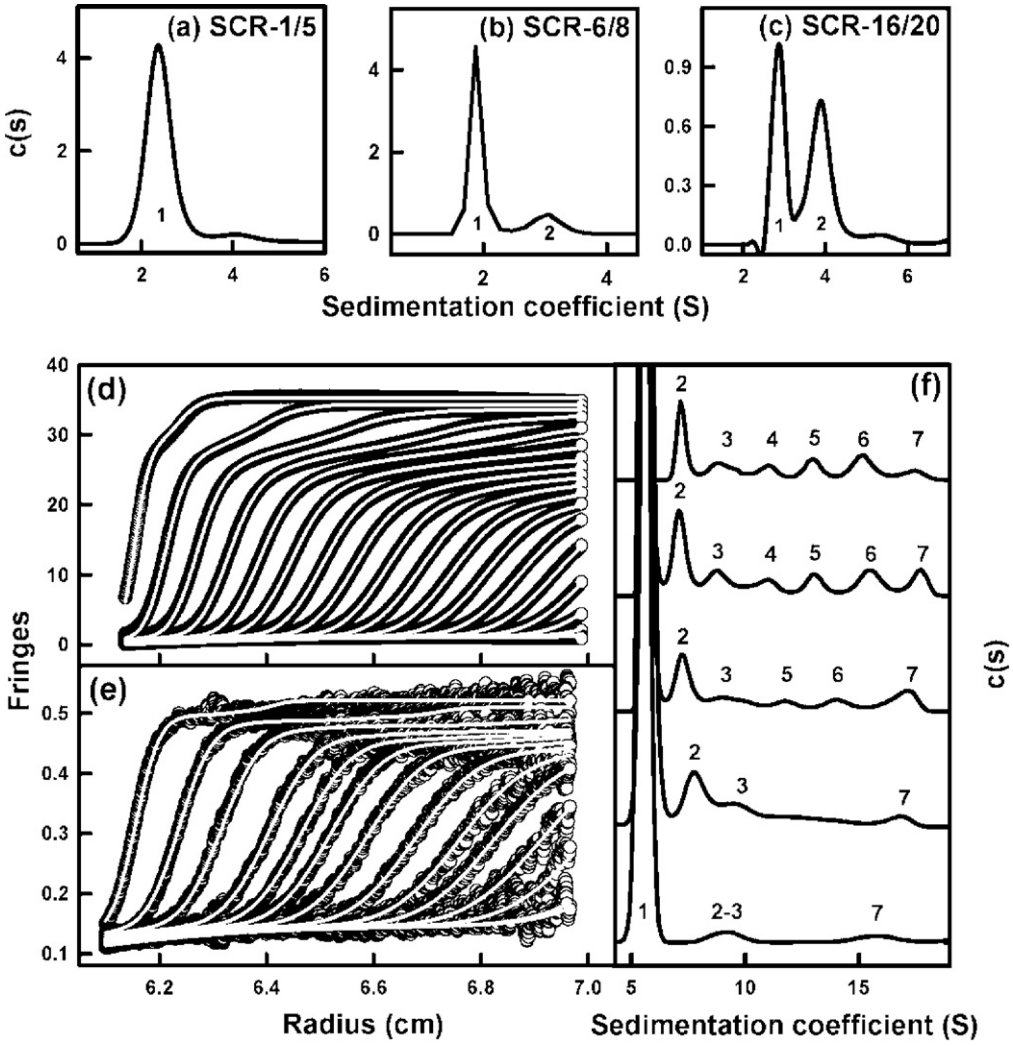

Fig. 2. Self-association of FH by analytical ultracentrifugation. The sedimentation velocity $c(s)$ distribution analyses are shown for four FH proteins. For the SCR-1/5 fragment in (a), a single $s_{20,w}$ peak is seen at 2.4 S, indicating monomer. For SCR-6/8 (His402) in (b), two $s_{20,w}$ peaks are seen at 2.0 S and 3.2 S, indicating a predominant monomer and small amounts of dimer. For SCR-16/20 in (c), two $s_{20,w}$ peaks are seen at 2.9 S and 3.8 S, indicating both monomer and dimer. In (d) for wild-type FH at 5.9 mg/ml, a more rapidly sedimenting component is seen at the top of the boundaries, while in (e) this feature is less apparent for FH at 0.17 mg/ml. In (f), in the five $c(s)$ analyses for FH between 0.17 mg/ml and 5.9 mg/ml, the monomer peak is denoted by 1, and the FH oligomers are labelled from 2 to 7. In these $c(s)$ plots, the FH dimer (peak 2) reaches 7% of the intensity of peak 1 for the top trace.

Adapted from Fernando et al. (2007), Okemefuna et al. (2008) and Nan et al. (2008a,b).

from which the K_D value is obtained (Okemefuna et al. 2010a,b). The use of all three methods together is advantageous to reduce the experimental uncertainties inherent by the use of a single method.

Self-association of Factor H

A molecular understanding of the FH interactions with its ligands requires the K_D values for each FH–ligand complex. Given that FH self-associates with a μM K_D value that is comparable to the K_D values for its FH–ligand complexes (Table 1), an understanding of FH self-association is relevant to FH–ligand studies. Accurate FH concentrations are required for K_D determinations. There are literature discrepancies in the determination of FH concentrations from 280 nm absorbance measurements. The original FH sequence showed that five of the nine putative N-glycosylation sites in FH were occupied, together with one more of the three remaining sites, and that SCR-4 was not glycosylated (Ripoche et al. 1988). It is now known from mass spectrometry that eight of the nine glycosylation sites in FH are occupied, and the non-glycosylation of SCR-4 was confirmed (Fig. 1a) (Fenaille et al. 2007). From this knowledge and the FH sequence, the FH molecular mass is calculated as 154.4 kDa and the predicted FH absorption coefficient at 280 nm (1%, 1 cm path length) is revised to be 16.2 (Perkins 1986). The latter is high for reason of the conserved Trp residue found in most SCR domains. Other groups work with a 20% higher absorption coefficient of 19.5 (Hakobyan et al. 2008) or a 12–23% lower value of 14.2 or 12.4 (Sim and DiScipio 1982; Pangburn et al. 2009). A value of 16.0 is used by the Edinburgh group (Schmidt et al. 2011). The value of 16.2 used in our work is conveniently close to the mean of the three experimental determinations.

The self-association property of FH was first quantitatively identified by X-ray scattering in 1991 (Perkins et al. 1991). At the comparatively high FH concentration of 2 mg/ml (13 μM), the FH molecular weight was almost doubled when this was compared to the scattering intensities from standards. Self-association was disputed when DiScipio (1992) argued from the single peak seen by gel filtration and single electron microscopy images of FH that FH was monomeric; that study did not consider the possibility of an equilibrium between monomer and dimer forms. Scattering studies of gel-filtered FH in a wide range of concentrations

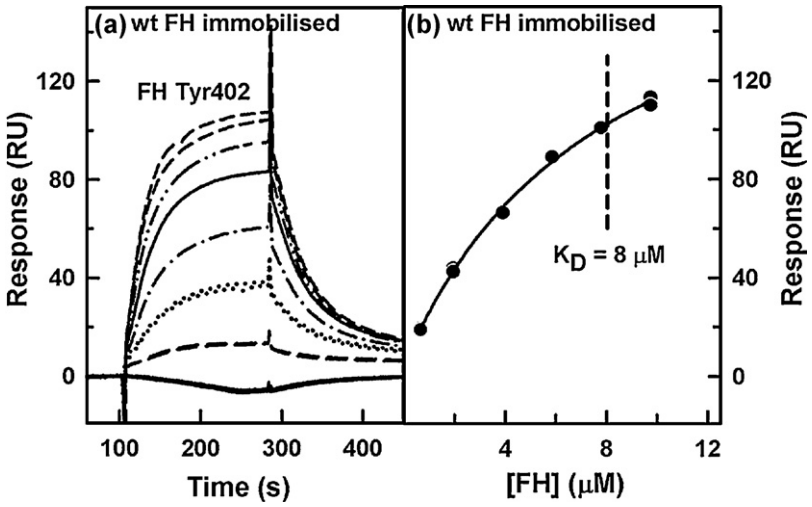

Fig. 3. Self-association of FH by surface plasmon resonance. (a) The ligand was 150 RU of wild-type heterozygous FH immobilised on a CM5 chip. The analyte was a homozygous FH Tyr402 sample at seven concentrations between 0 μM and 9.7 μM in 10 mM HEPES, 137 mM NaCl buffer, pH 7.4. (b) The binding affinity was fitted to a 1:1 binding model using the maximum response values in (a), resulting in a K_D value of 8.0 μM with a χ^2 value of 2.6 RU^2 (vertical dashed straight lines).
Taken from Nan et al. (2010).

of 0.7–14 mg/ml (5–90 μM) also suggested monomer (Aslam and Perkins 2001). The FH monomer issue appeared to be settled until more sensitive scattering and ultracentrifugation experiments with the FH SCR-6/8 fragment revealed a monomer–dimer equilibrium with a K_D of 40 μM (Fig. 2b) (Fernando et al. 2007). The FH SCR-16/20 fragment also showed a monomer–dimer equilibrium with a K_D of 16 μM (Fig. 2c) (Okemefuna et al. 2008). No dimer was seen for SCR-1/5 (Fig. 2a) (Okemefuna et al. 2008), while the deglycosylated SCR-12/13 fragment showed 20% dimer formation (Schmidt et al. 2010). Even though self-association may be artefactual, possibly caused by working with fragments or deglycosylation, the observation of dimerization in SCR-6/8 and SCR-16/20 prompted the re-examination of native FH. The possibility of at least two different self-dimerisation sites in FH led to the prediction that an indefinite set of FH oligomers could be formed through the alternate daisy-chaining of these dimerization sites. The presence of FH monomers and dimers and smaller amounts of larger species ranging up to heptamers was directly confirmed using size-distribution analyses $c(s)$ of the sedimentation velocity data (Fig. 2d–f). The $c(s)$ analyses comprised a new ultracentrifugation method that successfully resolved these FH oligomers (Nan et al. 2008a). The molecular modelling of FH oligomeric structures verified the observed sedimentation coefficients of these $s_{20,w}$ peaks 2–7. At the same time, improvements in X-ray scattering technology enabled small FH concentration dependences between 1 and 5 mg/ml to be identified that were missed in the Aslam and Perkins (2001) study. Overall, sedimentation equilibrium showed that, below 1 mg/ml, FH could be fitted as a reversible monomer–dimer equilibrium with a K_D of 28 μM (Nan et al. 2008a). Above 1 mg/ml FH, as evidenced by gel filtration of stored FH, oligomer formation became irreversible.

The question arises of whether FH self-association seen in the test-tube also occurs in plasma. In typical 0.2–0.8 mg/ml plasma concentrations of FH, the K_D value of 28 μM means that 5–14% of FH will be dimeric and higher if no other factors influence this equilibrium. The stability of these FH oligomers was therefore tested by variation of the buffer. The use of different NaCl concentrations (50 mM, 250 mM) and different pH 3 and pH 9 confirmed that these FH oligomers existed in all these conditions, with more oligomer being seen in low salt (Okemefuna et al. 2009a). Conformational changes in FH were also detected, when its overall length increased with NaCl concentration. Thus FH self-association is a robust property that is likely to prevail in the 70 mg/ml environment of plasma proteins at pH 7.4. The literature showed a varied acceptance of FH self-association. Thus the Jena group reported FH self-association with SCR-1/7 using surface plasmon resonance (Oppermann et al. 2006). The Helsinki group saw dimers of FH SCR-15/18 and SCR-15/20 by non-reducing SDS-PAGE and in the crystal structure of SCR-19/20, although dimers seen in a crystal would not generally be regarded as evidence for dimerization in solution (Jokiranta et al. 2000, 2006). The Texas group noted some propensity for self-association by sedimentation equilibrium (Pangburn et al. 2009). In distinction, the Edinburgh group did not see dimer in SCR-19/20 by NMR (Herbert et al. 2006), although NMR is insensitive to dimer formation. The Edinburgh group also reported FH at 1 mg/ml to be monomer by dynamic light scattering "with little propensity to self-associate" (Schmidt et al. 2011), although light scattering is unable to resolve monomer and dimer if their overall shapes are similar (Nan et al. 2008a).

The proper interpretation of FH–ligand experiments requires allowance for FH self-association. Even though this will potentially complicate data interpretation, it can sometimes simplify these. Given that the main evidence for FH self-association is from the ultracentrifugation $c(s)$ analyses and scattering concentration dependences, other methods have now been used to strengthen the evidence for FH self-association. Thus, FH oligomers have been seen using homozygous FH from genotyped donors (Nan et al. 2010, 2011), hence ruling out heterozygosity as the cause of oligomers. Mass spectrometry also revealed FH dimers and trimers. Surface plasmon resonance showed that homozygous FH in solution self-associated with immobilised heterozygous FH with a K_D value of 8 μM, although our subsequent more detailed studies (unpublished) show that the actual K_D value is larger (Fig. 3). FH self-association is summarised in Fig. 4a.

Interactions of Factor H with the C3 proteins

C3 (190 kDa) at 1.3 mg/ml (7 μM) is the central complement protein, and its plasma concentration rises by 50% in acute phase conditions. During circulation in blood, the thioester group in C3 is slowly hydrolysed to form C3u, alternatively known as C3(H_2O). C3u participates in C3 convertase formation to enable C3 to be rapidly cleaved to functionally active C3b and a small anaphylatoxin C3a. Cleavage induces a conformational change in this compact 13-domain protein, in which C3d (the TED domain)

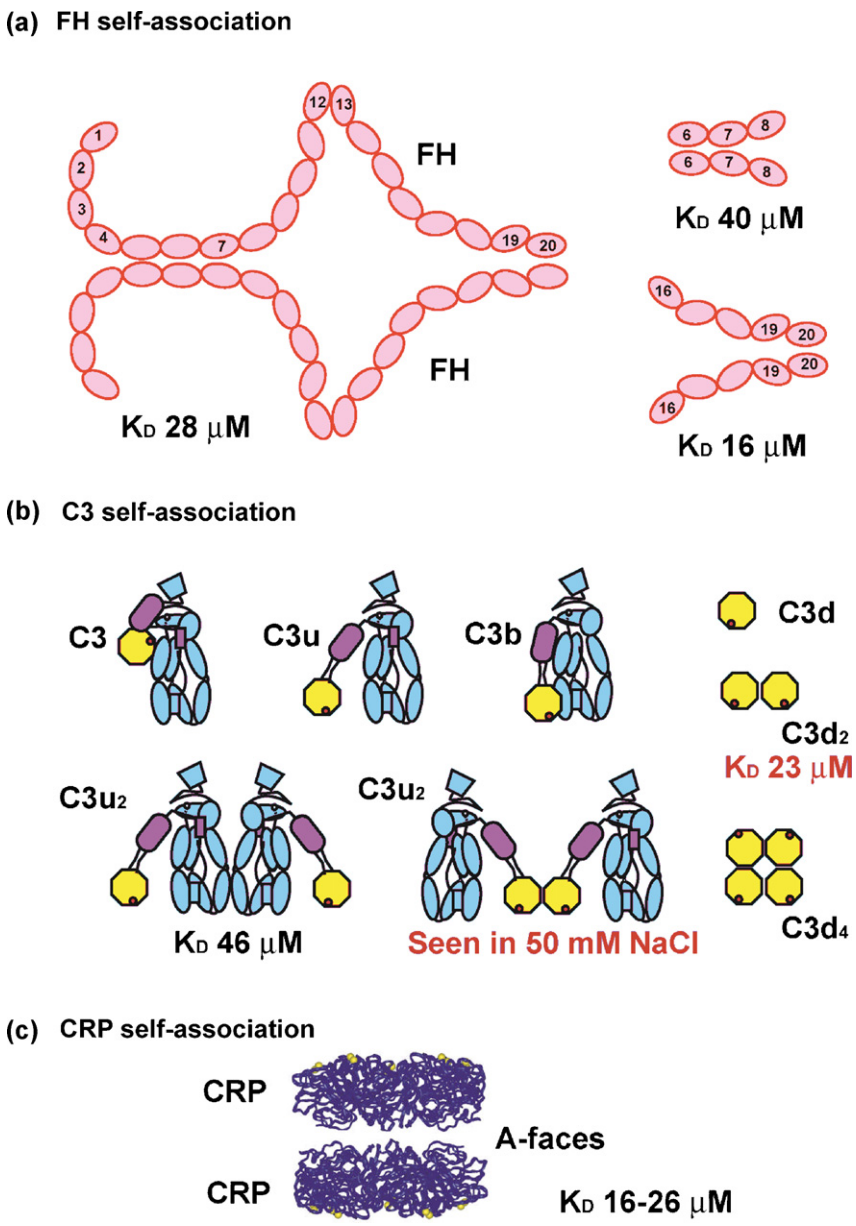

Fig. 4. Cartoon of FH, C3 and CRP self-association. The current understanding of self-association is depicted, following the colour scheme in Fig. 1b. (a) A putative FH dimer is shown that self-associates through two dimer sites at SCR-6/8 and SCR-16/20. Higher FH oligomers can form through the daisy-chaining of these dimer sites. Adapted from Fernando et al. (2007), Okemefuna et al. (2008) and Nan et al. (2008a,b). (b) Schematic domain diagrams for C3, C3u and C3b that show the different positions of the TED and CUB domains in these three proteins. The ANA domain present in C3 and C3u but not in C3b is also shown. Both C3 and C3u form back-to-back dimers with a K_D of 46 μM as depicted. In low salt (red font), C3 and C3u undergo further self-association, and this resembles the self-association of C3d (TED domain) in the same buffer (data in red font). Adapted from Li et al. (2008, 2010). (c) CRP pentamers self-associate to form decamers through contacts between its A-faces. Adapted from Okemefuna et al. (2010a). (For interpretation of the references to color in this figure legend, the reader is referred to the web version of the article.)

(Fig. 1b) moves from one end of the C3 structure to the other end to expose an internal thiolester group within this domain (Janssen et al. 2005). This exposed thioester of C3b is able to form a covalent bridge with pathogenic and host cell surfaces to label these for complement attack. C3b bound to host cells is inactivated by Factor I protease with FH as the regulatory cofactor to result in the cleavage of C3b to form the TED domain (also known as C3d) and C3c. C3b itself dimerises with the Bb protease fragment of Factor B to form the C5 convertase. High resolution crystal structures are known for C3, C3a, C3b, C3c and C3d and their macromolecular complexes with ligands such as FH SCR-1/4, Factor B and complement inhibitors (Gros et al. 2008; Rooijakkers et al. 2009; Forneris et al. 2010). The solution properties of the C3 proteins and their interactions with ligands such as FH are less well known.

The C3d fragment shows salt-dependent oligomeric properties. In low salt (50 mM NaCl buffer), X-ray scattering showed concentration-dependent R_G values that initially suggested a monomer–dimer K_D value of 23 ± 3 μM (Table 1) (Gilbert et al. 2005; Perkins and Furtado 2005). Scattering modelling resulted in good curve fits for monomers at low concentrations when dissociation into monomers had occurred (Gilbert et al. 2005). Subsequent analytical ultracentrifugation $c(s)$ analyses and sedimentation equilibrium fits showed that, in 50 mM NaCl, C3d exhibited a monomer–dimer–trimer equilibrium rather than a monomer–dimer equilibrium (Li et al. 2008). In fact, the $s_{20,w}$ values suggest that a monomer–dimer–tetramer equilibrium cannot be ruled out (Figs. 4b and 5b). In contrast, in physiological 137 mM NaCl buffer, C3d is observed to be monomeric only in $c(s)$ plots.

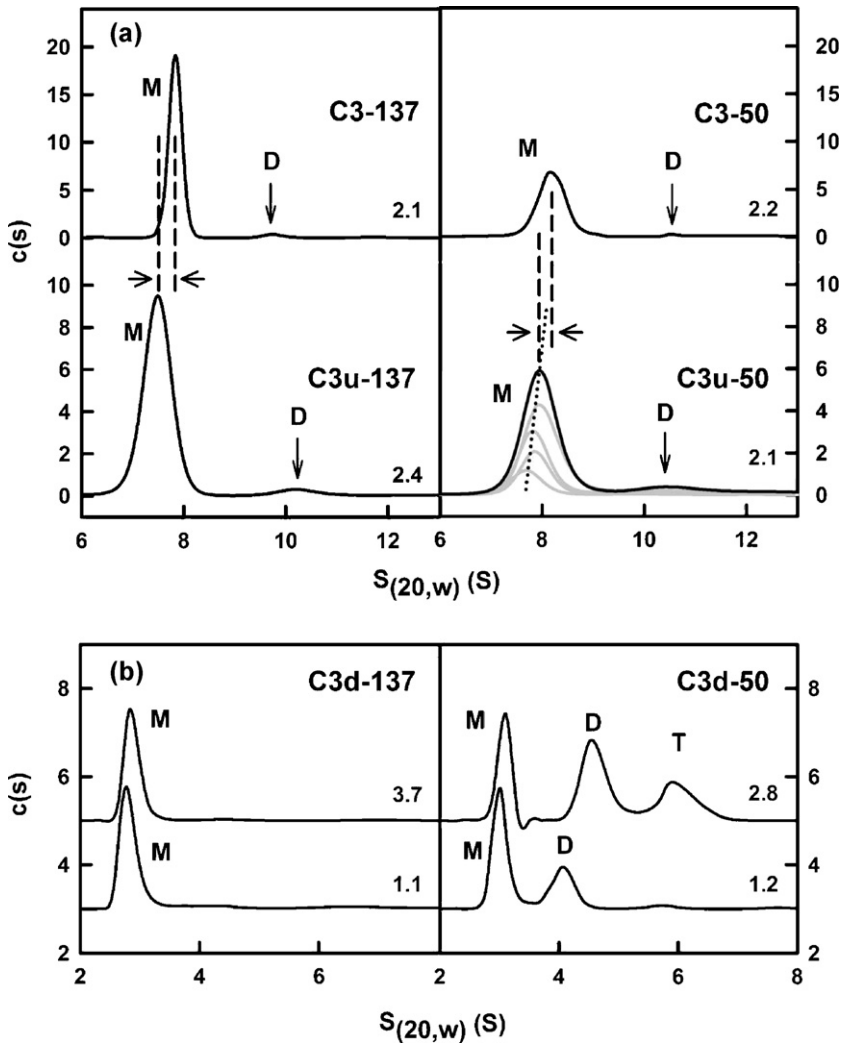

Fig. 5. Multimerisation of C3, C3u and C3d. The sedimentation velocity $c(s)$ distribution analyses are shown for three C3-related proteins. (a) The $c(s)$ distributions for C3 and C3u in 137 mM (left) and in 50 mM (right) NaCl buffers. A major C3 monomer $s_{20,w}$ peak is visible at 7.85 S in 137 mM NaCl, which is shifted to 8.02 S in 50 mM NaCl. This peak is unchanged with concentration in 137 mM NaCl, but shifts with concentration in 50 mM NaCl. A second $s_{20,w}$ peak corresponding to discrete C3 dimers is visible at 11.2 S. A major C3u monomer $s_{20,w}$ peak is visible at 7.44 S in 137 mM NaCl, which is shifted to 7.66 S in 50 mM NaCl. This peak is unchanged with concentration in 137 mM NaCl, but shifts with concentration in 50 mM NaCl. A second $s_{20,w}$ peak corresponding to discrete C3 dimers is visible at 11.5 S. The change in sedimentation coefficient between C3 and C3u is shown by the vertical dashed lines. (b) The $c(s)$ size distributions for C3d at 1.1 mg/ml and 3.7 mg/ml in 137 mM NaCl (left) and 50 mM NaCl (right) is shown. In 137 mM NaCl, a single species at 2.9 S is seen and was designated as a monomer. In 50 mM NaCl, two or three $s_{20,w}$ peaks are seen at 1.2 mg/ml and 2.8 mg/ml, and are designated as M (monomer), D (dimer) and T (trimer/tetramer) in increasing order of S values.
Adapted from Li et al. (2008, 2010).

This outcome warns against the use of 50 mM NaCl for FH–C3 experiments. Low salt is advantageous in promoting weak ionic interactions that will increase the amount of complex formed for experiments. However, low salt can promote binding artefacts, because inappropriate ionic interactions become more significant and can lead to non-physiological complex formation.

The oligomeric properties of C3 and C3u were likewise established in both 50 mM and 137 mM NaCl buffers using analytical ultracentrifugation and X-ray scattering (Li et al. 2010). The $c(s)$ sedimentation coefficient analyses identified two distinct dimerization events for each protein (Fig. 5a). A low amount of a fast dimerization at 8 S, which leads to a concentration-dependent single peak known as a reaction boundary, was observed only in 50 mM NaCl for C3 and C3u and not in 137 mM NaCl. Given that C3d is equivalent to the TED domain, and shows the same salt-dependent behaviour as C3 and C3u, the fast dimerization is most likely to arise from self-association involving the TED domain (Fig. 4b). Minor amounts of a second slow dimerization were observed for both C3u and C3 at about 11 S in both buffers. The monomer and dimer $s_{20,w}$ peak intensities lead to a K_D of 38 ± 16 μM for C3u and C3 in 50 mM NaCl, and a K_D of 46 ± 15 μM for C3u and C3 in 137 mM NaCl for this slow dimerization (Table 1). This second dimerization event may correspond to the C3b dimer observed in one of the C3b crystal structures (Fig. 4b). This C3b dimer is to be distinguished from the C3b dimer of the C5 convertase when one C3b molecule binds to another C3b molecule through its thioester group. The 11 S sedimentation coefficient of this second dimer $s_{20,w}$ peak was validated by calculation using a C3b dimer seen in one of the C3b crystal structures. The R_G concentration dependences seen by X-ray scattering supported the $c(s)$ analyses, although scattering is not able to identify directly the oligomeric species that were present. In further analyses, the molecular modelling of the scattering curves showed that the TED/CUB domains in monomeric C3u were extended into solution. This TED/CUB conformation is intermediate, but distinct from, that between those found in C3 and C3b (Fig. 4b). In reflection of this conformational change, the sedimentation coefficients of C3u are slightly lower than those of C3 (Fig. 5a).

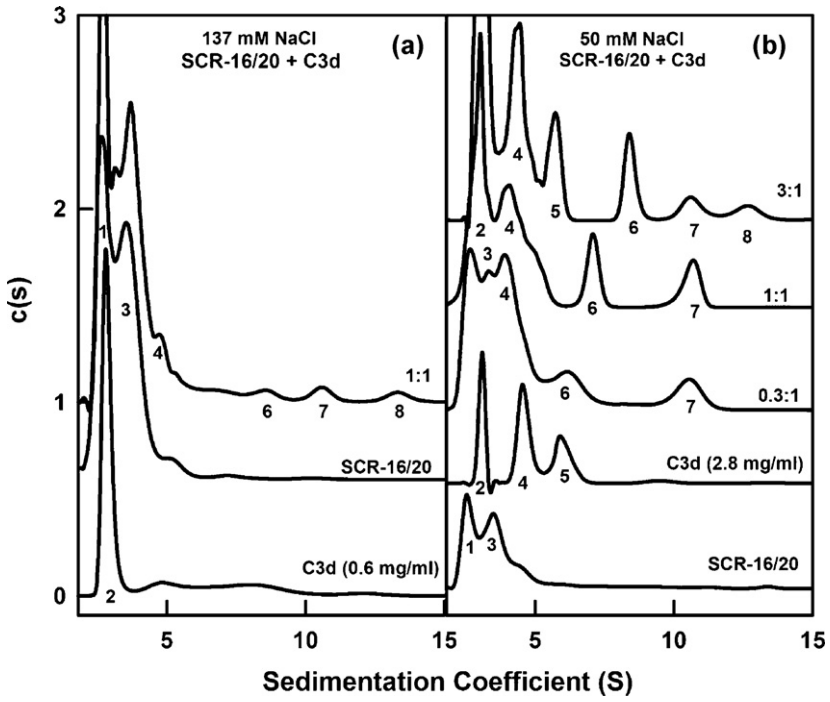

Fig. 6. Interaction between SCR-16/20 and C3d by analytical ultracentrifugation. The $s_{20,w}$ peaks 1 and 3 correspond to the monomer and dimer of SCR-16/20 (Fig. 2c). The $s_{20,w}$ peaks 2, 4 and 5 in 50 mM NaCl correspond respectively to the monomer, dimer and putative trimer/tetramer from C3d (Fig. 5b). (a) The $c(s)$ analyses from experiments in 50 mM NaCl buffer with mixtures of SCR-16/20 and C3d showed two extra peaks 6 and 7 at large S values at low stoichiometric ratios, to be replaced by three peaks 6, 7 and 8 at high ratios. (b) The corresponding experiment in 137 mM NaCl buffer showed that, although the peaks 4 and 5 from C3d have disappeared (Fig. 4), peaks 6, 7 and 8 are still visible.

Adapted from Okemefuna et al. (2009a,b).

FH binds to two dominant different locations in C3b, with one C3b site at SCR-1/4 and the other C3b site at SCR-19/20 (Schmidt et al. 2008). The SCR-1/4 site in C3b lies between the CUB/TED domains and the MG domains (Fig. 1b). FH also binds C3d at the SCR-19/20 site (Bhattacharjee et al. 2010). Biophysical solution studies of these interactions were initiated with the SCR-16/20 fragment and C3d, and working with both 50 mM and 137 mM NaCl buffers (Okemefuna et al. 2009b). Ultracentrifugation showed that as many as eight $s_{20,w}$ peaks were observed in both buffers in the size distribution $c(s)$ plots on mixing C3d with SCR-16/20 (Fig. 6), even though only three $s_{20,w}$ peaks were expected for the two unbound proteins and their complex. This outcome showed that the C3d–FH interaction site does not block the interaction sites responsible for the formation of C3d oligomers, unlike the case of the CR2 SCR-1/2 complex with C3d (Gilbert et al. 2005). The concentration dependence of the eight $s_{20,w}$ peaks, such as peak 6 in Fig. 6b, showed that the interaction was a weak one with comparatively rapid on/off rates. At that time, by assuming a monomer–dimer equilibrium for each of SCR-16/20 and C3d, the eight $s_{20,w}$ peaks were originally explained in terms of putative C3d dimers and SCR-16/20 dimers that associated in alternation with each other to form oligomers with stoichiometries of 1:1 to 8:8. The occurrence of multimers was confirmed by surface plasmon resonance. Thus K_D values of 1 μM and 2.4 μM were determined in 50 mM and 137 mM NaCl respectively for a 1:1 complex of C3d and SCR-16/20. Further intensity changes were seen at higher C3d analyte concentrations that reflected higher multimerisation. The two recent crystal structures of the C3d–SCR-19/20 complex now clarify these results (Kajander et al. 2011; Morgan et al. 2011), although neither study acknowledged our 2009 surface plasmon resonance and ultracentrifugation study of this interaction. The Helsinki crystal structure reported a 2:1 complex with two C3d bound per SCR-19/20 at two distinct sites on SCR-19/20. Our observation of eight peaks for the SCR-16/20 and C3d mixtures may be explained in terms of a series of eleven distinct monomers and oligomers deduced from that crystal structure (ten are shown in Fig. 7b). The Edinburgh crystal structure revealed only a 1:1 complex between C3d and SCR-19/20, and this leads to a prediction of eight distinct monomer and oligomer forms for the C3d mixture with SCR-16/20.

The 2009 FH–C3d study provided insight into complement regulation. After host-cell bound C3b is inactivated by Factor I cleavage into C3c and C3d, C3d will be left bound through its thioester group to the host cell surface. When C3b activation levels are high, larger amounts of C3b will be deposited and inactivated on host cell surfaces, hence increasing the amount of available C3d. Consequently host cells will present significant levels of C3d-coated surfaces. Equivalent high levels of C3d will not be formed on foreign cells because FH is not expected to bind to their surfaces. The ability of C3d and FH to form multimeric complexes at host cell surfaces will enable even more FH to bind to host cells in order to offer additional complement regulatory protection under chronic inflammatory conditions.

FH–C3b complex formation will be incomplete in plasma. When C3 is activated to C3b in body fluids, only small amounts of C3b will form. The C3b concentration is expected to be low at μg/ml levels (0.1 μM). It could be argued that the "local" C3b concentration might be quite high over a very short period. However it is not possible that equimolar amounts of 0.8 mg/ml FH and 1 mg/ml C3b (5 μM) will co-exist *in vivo*. The K_D values for the FH–C3b and FH–C3u interactions lie in a range of 0.59 to 2.9 μM in 137–150 mM NaCl (Table 1). If theoretically equimolar amounts of FH (0.8 mg/ml) and C3b/C3u (1 mg/ml) occur at 5 μM in plasma, 48–71% of complex will be formed, meaning that a significant proportion of FH and C3b/C3u will be uncomplexed. If FH is at 5 μM and C3b is at 0.1 μM, much lower levels of 2% complex will be formed. Stronger complex formation occurs in 50 mM NaCl, showing the role of electrostatic forces in stabilising the complex (Table 1). This result for FH is confirmed by the FH fragments. Two studies of SCR-1/4

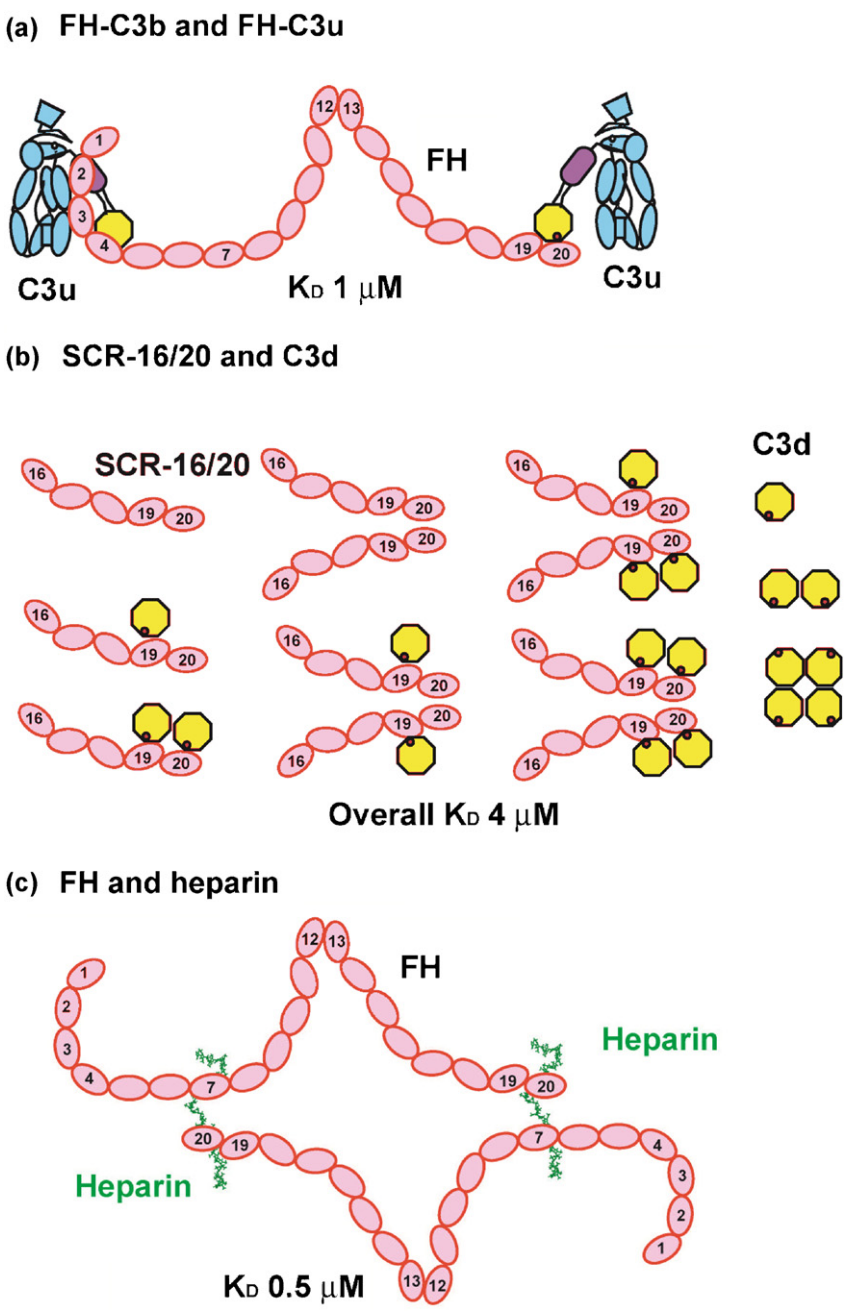

Fig. 7. Cartoon of FH interactions with its ligands. The current understanding of how FH interacts with its major ligands is depicted. (a) C3u or C3b will bind to SCR-1/4, and both will also bind to SCR-19/20 through its TED (C3d) domain. A two-site model is shown with a 2:1 stoichiometry. Many groups consider that one molecule of FH wraps itself around C3b to form a 1:1 complex. (b) SCR-16/20 and C3d interact with each other to form a series of multimers that are seen in the *c*(*s*) analyses (Fig. 6). A schematic outline of possible complexes based on C3d binding to each of SCR-19 and SCR-20 is shown. (c) FH interacts with anionic oligosaccharides at SCR-7 and SCR-20. In solution, a 2:2 complex is formed (peak 2 in Fig. 8b) as well as others.

binding to C3b gave comparable K_D values in a range of 9.8–13.5 μM (Table 1), indicating that 5 μM of SCR-1/4 would only be 22–27% bound to C3b. Three studies of SCR-19/20 binding to C3b gave comparable K_D values in a range of 0.54–5.4 μM (Table 1), indicating that 5 μM of SCR-19/20 would only be 37–72% bound to 5 μM C3b. Similar K_D ranges are seen also for SCR-19/20 binding to C3d in 137–150 mM NaCl (Table 1). Even though there can be a 2-fold to 10-fold variability in the individual K_D values measured in different laboratories, this variability is attributable to the chip surface used for measurements and the use of different protein preparations, which can alter between laboratories or even within them (Morgan et al. 2011). The overall view of these three single-site or double-site FH interactions is that only about 50% FH–C3b complex is expected to be formed at best in body fluids. In plasma/serum, C3b is broken down very quickly to iC3b, indicating that a C3b–FH complex has formed. Kinetics are important here: it was not possible to include extensive kinetic analysis in this review, but the potential importance of the fast on/off rates for the FH–C3b complex are consistent with the μM K_D values. In addition, given that there is no major enhancement in the K_D value for intact FH compared to those for the FH fragments, this suggests that the two C3b binding events may be independent of each other (Fig. 7a). Electron microscopy suggested that C3b only binds to one end of FH (DiScipio 1992). In distinction, much of the FH–C3b literature discuss alternative structural models in which FH becomes wrapped around C3b in a 1:1 complex, the contacts being mediated by both

SCR-1/4 and SCR-19/20 in intact FH (Kajander et al. 2011; Morgan et al. 2011).

Interaction of Factor H with heparin

FH regulates surface-bound C3b activity on host cells by recognising polyanionic structures such as heparan sulphate on these surfaces, thereby inhibiting complement activation. Heparin is an analogue of heparan sulphate. Heparin fragments of sizes dp6–dp36 (dp: degree of polymerisation, corresponding to 3–18 iduronate and glucosamine disaccharide units) have a semi-rigid and extended conformation that is pre-formed and optimal for binding to protein targets such as FH without major conformational changes (Fig. 1) (Khan et al. 2010). These heparin solution structures became progressively more bent with increased size. Heparan sulphate fragments dp6–dp24 have also been studied in a predominantly unsulphated form. The smaller ones dp6–dp16 revealed a longer and more bent structure than heparin. The longer ones dp18 and dp24 exhibited multiple structures and a higher degree of flexibility than the corresponding heparin fragments (Khan et al. 2011).

Heparin is often used as an analogue for heparan sulphate, and interacts with FH primarily at SCR-7 and SCR-20 (Fig. 1). The first estimates of K_D values in 50–100 mM NaCl buffer suggested values of 9 μM or 9.2 nM (Table 1). The FH SCR-6/8 fragment showed a bent SCR domain arrangement that binds heparin dp10 tightly in 137 mM NaCl buffer by ultracentrifugation $c(s)$ analyses (Fernando et al. 2007). This tight binding placed an upper limit of 14 μM for the K_D for the SCR-6/8 interaction with dp10. X-ray scattering suggested that SCR-6/8 with dp10 changed conformation or formed oligomers. This work was extended to full-length FH by studying the effects of dp6–dp36 using 1:1 mixtures of FH–heparin by X-ray scattering and analytical ultracentrifugation (Khan 2011). The X-ray radius of gyration R_G of FH decreased slightly for dp6 and dp12, which is explained by the removal of FH self-association through heparin binding. Since the FH monomer–dimer K_D value is 28 μM, this shows that the K_D for the FH–heparin interaction is below 28 μM. With dp18–dp36, the R_G values increased, and the scattering curves showed that compact FH–heparin oligomers had formed. The results were confirmed by ultracentrifugation, when the 12–15% of FH oligomers became 61–63% oligomers with dp30–dp36 (Fig. 8a). The $c(s)$ peaks ranged from dimeric to decameric FH–heparin complexes with sedimentation coefficients that were smaller than those for FH to indicate that larger structures had been formed with heparin (Fig. 8b). The 61–63% of FH oligomers correspond to a K_D value of about 0.5 μM for the interaction with dp30 and dp36. In addition, computer modelling showed that no major conformational change in FH occurred when FH was crosslinked by heparin to form dimeric, trimeric, tetrameric and pentameric rings. Instead, heparin inserted itself between FH molecules to form larger structures (Fig. 7c). Thus at μM concentration levels of FH in plasma, FH is able to interact with heparin at two independent sites.

In theory, the combination of two separate FH–heparin weak binding events with μM K_D values on the one molecule will become a higher affinity with an overall K_D of pM (the product of the two individual K_D values) (Jencks 1981). In practice, a full enhancement in affinity is not seen. Nonetheless, depending on the surface density of heparin-like structures and the flexibility of FH, the independent binding of both heparin sites on FH to a single host cell surface will strengthen the overall interaction. Therefore the bivalency of the FH–heparin interaction would be a major advantage for its regulatory role. Bivalency would facilitate the selective binding of FH to host cells so long as the host cells displayed multimeric

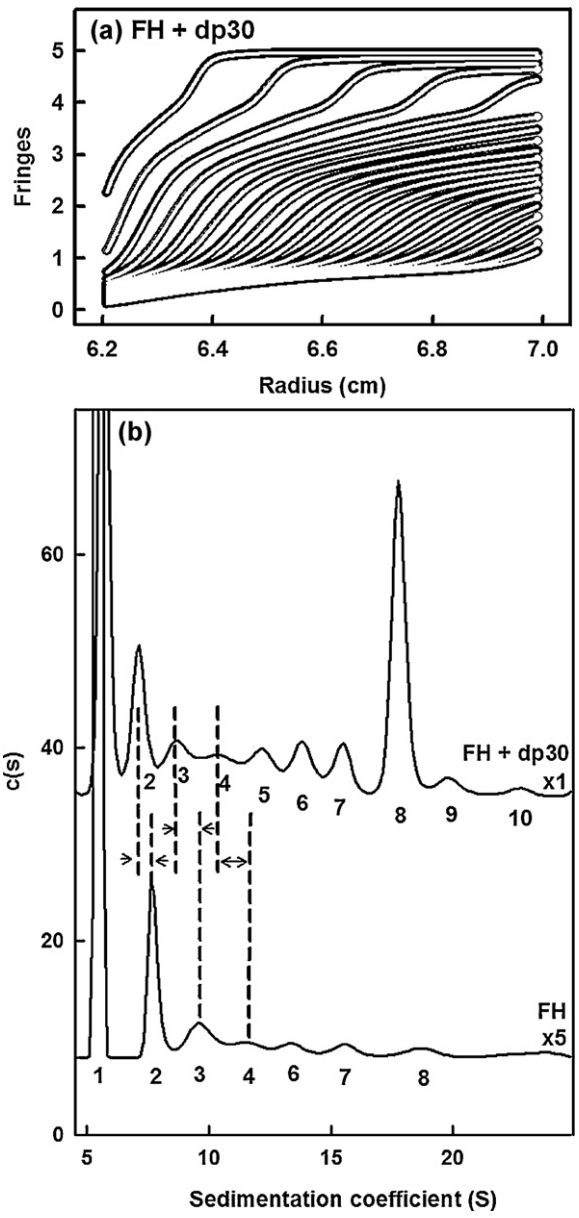

Fig. 8. FH–heparin interaction by analytical ultracentrifugation. (a) FH at 1.08 mg/ml (7 μM) was studied in the presence of a 1:1 molar ratio of dp30. The experimental velocity scans are shown in black, and the fits are shown in white. A more rapid sedimentation is observed at the top of the scans that corresponds to the FH–heparin oligomers. (b) The $c(s)$ analyses for FH alone and the FH–dp30 heparin mixture are shown. The FH monomer $s_{20,w}$ peak is labelled as 1, and the FH oligomer $s_{20,w}$ peaks (dimer onwards) are denoted by 2–12 in increasing order of S values. The change in the sedimentation coefficients for peaks 2, 3 and 4 between FH and FH–dp30 is shown by the vertical dashed lines.
Adapted from Khan (2011).

polyanionic surfaces with an appropriate density of binding sites, unlike the pathogens that lack these multiple sites.

The relationship of heparin binding to disease remains to be elucidated in detail. Curiously, AMD is genetically related with a defective SCR-6/8 binding site, while aHUS is related with a defective SCR-19/20 binding site. In the context of AMD, three studies reported a higher affinity of heparin for the FH Tyr402 allotype compared to His402 (Herbert et al. 2007; Skerka et al. 2007; Ormsby et al. 2008). This implies that the weaker binding of FH His402 to host cell surfaces predisposes to AMD. A fourth study reported variable outcomes depending on the heparin preparation in use and its degree of sulphation (Clark et al. 2006). A fifth study reported

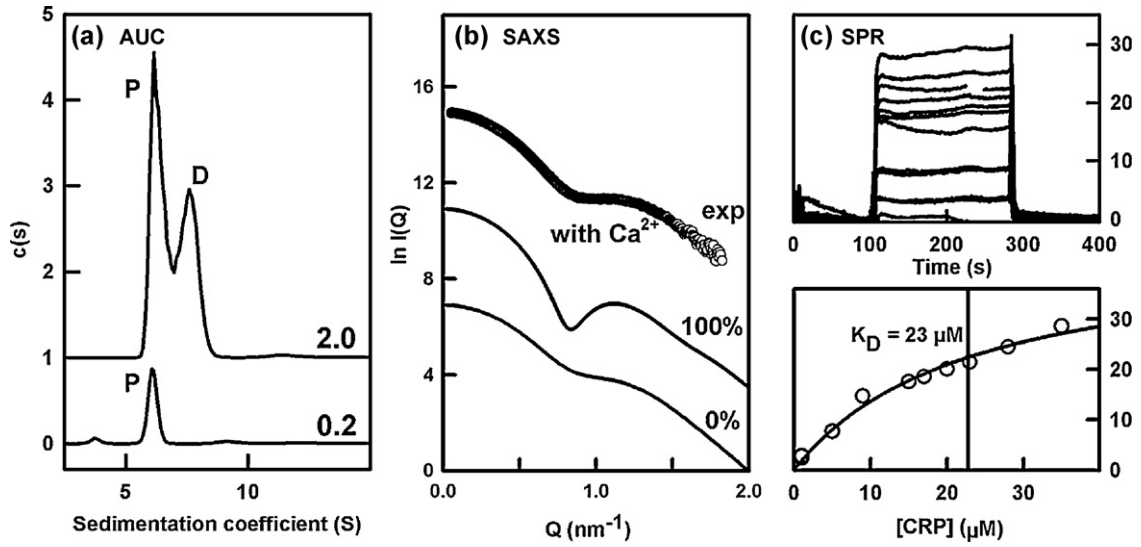

Fig. 9. Self-association of CRP by three methods. All the buffers contained 2 mM Ca^{2+} and 140 mM NaCl. (a) By analytical ultracentrifugation in solution, the pentamer and decamer forms were observed as two $s_{20,w}$ peaks, one at 6.4 S that corresponds to CRP pentamer at 0.2 mg/ml, and one at about 8 S that is a reaction boundary corresponding to a rapid equilibrium between pentameric and decameric CRP at 2.0 mg/ml. (b) By X-ray scattering, the experimental scattering curve at 2.7 mg/ml (upper) is a mixture of 41% of the CRP pentamer curve and 59% of the CRP decamer curve (lower two continuous lines). Fits of the lower two curves based on nine CRP concentrations gave a K_D value of 16 μM for the equilibrium. (c) Using surface plasmon resonance, a CRP analyte was flowed over immobilised CRP. The equilibrium analyses showed that saturation was approached from which a K_D value of 23 μM was determined (Table 1). The sensorgram showed that the on- and off-rates were rapid.

no significant binding difference between the Tyr402 and His402 allotypes (Yu et al. 2007).

Interaction of Factor H with C-reactive protein

CRP has five lectin-like subunits arranged as a flat disk with A- and B-faces. During the acute phase reaction, the plasma concentration of CRP (molecular mass 115 kDa) increases rapidly by over 1000-fold from 800 ng/ml in normal plasma to 0.5 mg/ml (from 7 nM to 4.4 μM). CRP binds ligands in a Ca^{2+}-dependent manner that reflects the 2.5 mM Ca^{2+} present in plasma (Hurwitz 1996). CRP binds to phosphorylcholine, as well as phosphoethanolamine, microbial surface proteins, chromatin and other ligands (Pepys and Hirschfield 2003). Ca^{2+} and phosphorylcholine bind to the B-face of CRP. These CRP–ligand interactions lead to the labelling of damaged or apoptotic cells and bacterial pathogens for recognition purposes. CRP activates the classical pathway of complement by binding to C1q at the A-face of CRP (Thompson et al. 1999). A FH–CRP interaction would be important if this regulates complement activation at CRP-coated damaged host cell surfaces.

The unravelling of the FH–CRP interaction was complicated by (i) FH self-association, (ii) CRP self-association (Fig. 4c), (iii) CRP denaturation, (iv) FH and CRP concentrations; (v) buffer composition. Prior to our re-investigation of this FH–CRP interaction (Okemefuna et al. 2010a,b), nine out of 11 earlier studies had concluded that FH and CRP formed a physiologically relevant complex, while two studies concluded that complex formation only occurred because denatured CRP was present. A critical evaluation of these 11 studies showed that the full physiological FH and CRP concentration range in plasma had not always been employed, 50 mM NaCl buffer and not 140 mM NaCl had sometimes been used, 2 mM Ca^{2+} had often been omitted from the buffer or was not specified, and two very different K_D values of about either 1 μM or 0.01 μM were measured previously for the same FH–CRP interaction.

The discrepancies in these 11 earlier FH–CRP studies now appear to be resolved (Okemefuna et al. 2010a,b). FH self-association with a monomer–dimer K_D value of 28 μM was noted above (Table 1). A CRP pentamer–decamer association with a comparable K_D value of 16–26 μM in 140 mM NaCl (Table 1) was identified by

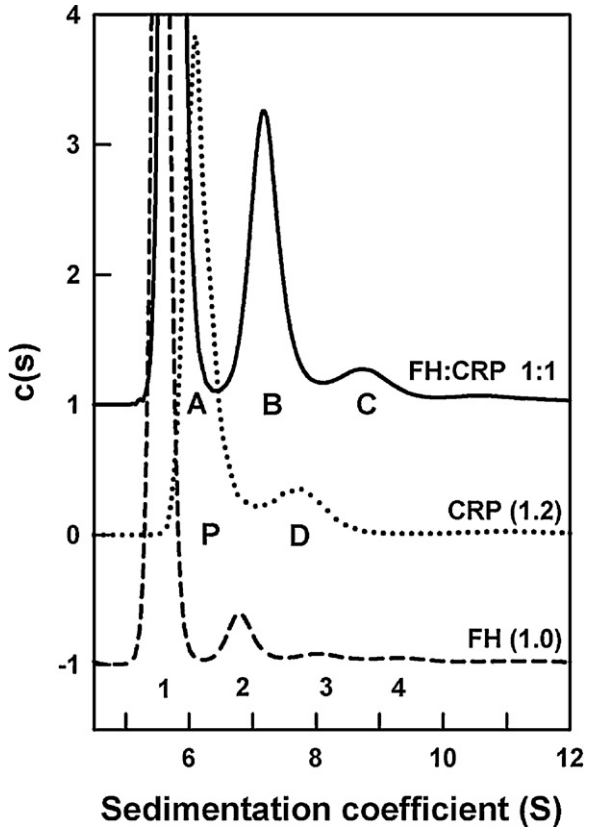

Fig. 10. Ultracentrifugation of FH, CRP and their complex. The $c(s)$ size-distribution analyses showed that free FH and CRP each formed oligomeric species, and these disappeared on mixing FH and CRP in buffers containing 2 mM Ca^{2+} and 140 mM NaCl. The data for FH at 1.0 mg/ml showed monomer (peak 1) and small amounts of dimer, trimer and tetramer (peaks 2–4) that are visible on the scale shown. The data for CRP at 1.2 mg/ml showed pentamer (P) and decamer (D). The 1:1 molar ratio mixture of FH and CRP showed that new peaks A, B and C formed at different S values from those of peaks 1, 2, 3, P and D, whereupon the higher oligomers of FH and CRP disappeared.
Adapted from Okemefuna et al. (2010b).

ultracentrifugation $c(s)$ analyses, X-ray scattering, and surface plasmon resonance (Fig. 9). Interestingly, CRP aggregated with immobilised CRP in 50 mM NaCl, adding another cautionary note about the use of 50 mM NaCl buffer. Because Ca^{2+} binds to CRP with a K_D of 30–60 μM (Table 1), 2 mM Ca^{2+} is required for full occupancy of the calcium binding sites in CRP. When insufficient Ca^{2+} is present, CRP partially dissociates into its protomers and denatures. Denatured CRP has a higher affinity for FH than native CRP, and this accounts for the low K_D values of about 0.01 μM for the FH–CRP interaction. In summary, a buffer with both 2 mM Ca^{2+} and 140 mM NaCl was essential for consistent results.

To clarify whether or not the FH–CRP interaction existed, FH and CRP mixtures were studied both in solution and on surfaces. Ultracentrifugation unexpectedly showed that the self-association of FH and CRP in these mixtures was suppressed (Fig. 10). The size distribution $c(s)$ plot for the 1:1 mixture showed the $s_{20,w}$ peaks for the expected unbound FH monomer and CRP pentamer, but with the reduction of the $s_{20,w}$ peaks for the FH dimer (peak 2) and CRP decamer (peak D) and the removal of the peaks 3 and 4 for the higher FH oligomers (Fig. 10). Two new peaks B and C appeared in the $c(s)$ plots. These were assigned to 1:1 and 2:1 complexes of CRP with FH. CRP and FH binding was also observed using surface plasmon resonance with FH-immobilised or CRP-immobilised chips respectively. Thus, using similar μM FH and CRP concentrations in the appropriate buffer, FH–CRP binding was determined to occur with a weak K_D of 4 μM (Okemefuna et al. 2010b).

Two CRP sites were identified in FH. This resembles the binding of FH to heparin (Fig. 11a) and to heparin and C3d (Fig. 11b). This was verified using surface plasmon resonance, where each of SCR-6/8 and SCR-16/20 bound to immobilised CRP, but SCR-1/5 did not (Okemefuna et al. 2010b). The removal of the FH dimers and higher oligomers after adding CRP indicated that both the FH self-association sites were blocked by CRP. Here, a notable difference in binding was seen between the wild-type allotype of SCR-6/8 (Tyr402) and the AMD-risk allotype of SCR-6/8 (His402) SCR-6/8 binding to native CRP. The K_D values were 4 μM (Tyr402) and 12 μM (His402). This difference provides molecular insight into an AMD-causative mechanism. In non-acute phase conditions, the resting CRP plasma concentration is low at 7 nM compared to FH at 7 μM, and CRP–FH will not interact because the K_D is 4 μM. During acute phase conditions, there will be sufficient CRP at 4.4 μM to interact with FH. Excessive complement damage on CRP-decorated damaged host cells would then be brought under regulatory control through FH binding to CRP at SCR-6/8 and SCR-16/20 (Fig. 11c). If the FH His402 allotype is present, this bivalent binding becomes less effective and FH is less able to regulate surface-bound C3b on host cells (Fig. 11d). During successive acute-phase reactions during a lifetime, the accumulation of damage caused by such a mechanism could contribute to the increased risk of AMD for individuals who are homozygous for FH His402. Interestingly, individuals who are homozygous for the FH His402 allotype show a 2.5-fold higher level of CRP in the RPE, as to be expected from this explanation (Johnson et al. 2006).

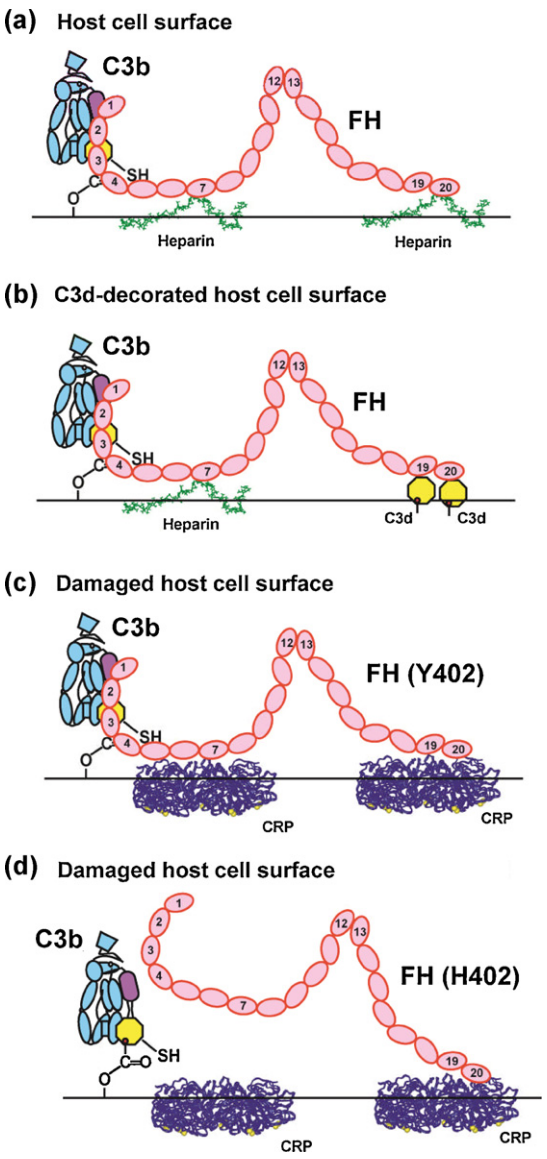

Fig. 11. Cartoon of three major FH interactions with host cell surfaces. The colour scheme follows that in Fig. 1b. (a) FH binds to heparan sulphate-coated host cell surfaces (represent here by heparin) through sites close to SCR-7 and SCR-19/20. This FH binding positions the SCR-1/4 domains in a conformation that binds readily to the FH binding site on C3b. The resulting C3b degradation to C3d and C3c will regulate complement activation at host cell surfaces. (b) In conditions of inflammation, the host cells accumulate C3d on its surface. This bound C3d provides additional FH binding sites that are able to recruit more FH to the host cell surface. This provides additional regulatory control when C3 is present at elevated levels during the acute phase response. (c) If the host cell surface is damaged and lipid is exposed, CRP is recruited to these host cells and binds wild-type FH (Y402) at both SCR-7 and SCR-20. The FH SCR-1/4 domains are again appropriately located to mediate the degradation of surface-bound C3b. (d) In contrast, FH (His402) is less able to regulate C3b degradation because of the weaker binding of SCR-7 (His402) to CRP. This is postulated to result in greater host cell damage. (For interpretation of the references to color in this figure legend, the reader is referred to the web version of the article.) Redrawn from Okemefuna et al. (2010b).

Interaction of Factor H with zinc

The accumulation of high bioavailable zinc concentrations in the subretinal pigment epithelial deposits (drusen) of the outer retina is associated with age-related macular degeneration (Lengyel et al. 2007). Bioavailable zinc corresponds to zinc that is weakly bound *in vivo* and therefore able to bind to targets with K_D values in μM ranges. Both microprobe synchrotron X-ray fluorescence and fluorescent zinc labels identified zinc concentrations as high as 200 ppm (several mM) in drusen. Even though much of this zinc will be tightly bound to proteins within drusen, the fluorescent probes prove the bioavailability of zinc. Elsewhere in the body, extracellular zinc levels as high as 300 μM is reached in the synaptic cleft. In plasma, zinc normally circulates at 12.5 μM where zinc is usually chelated. The K_D for zinc binding to human serum albumin is 1 μM, and 84% of plasma zinc is bound to this protein (Lu et al. 2008). Bioavailable plasma zinc occurs at 20–210 pM. Interestingly FH regulation is inhibited by zinc, which causes FH to aggregate (Perkins

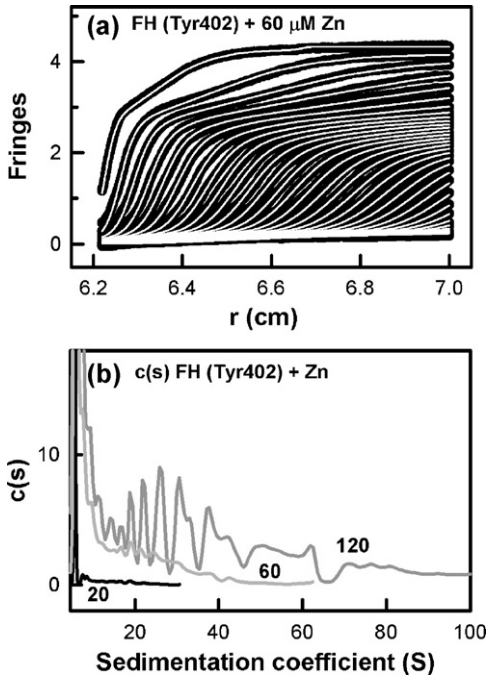

Fig. 12. The FH–zinc interaction by analytical ultracentrifugation. (a) The homozygous Tyr402 FH allotype at 0.7 mg/ml (5 μM) was titrated with zinc between 0.2 μM and 200 μM. In this sedimentation velocity experiment, only every tenth boundary scan is shown for clarity. The rapid sedimentation of aggregates at the top compared to monomeric FH is clearly visible in the scans. (b) The averaged $c(s)$ sedimentation coefficient distribution analyses from experiments at 20 μM, 60 μM and 120 μM zinc are compared with each other. The FH monomer peak is close to 5.7 S. Little aggregation at 20 μM zinc is seen. At 60 μM and 120 μM zinc, many more $c(s)$ peaks are seen between 20 S and 100 S. The zinc concentrations (μM) are denoted numerically.

Adapted from Nan et al. (2011).

et al. 1991), and this observation prompted a further investigation of the FH–zinc interaction.

Zinc-induced FH self-association was studied by X-ray scattering and analytical ultracentrifugation side-by-side with FH activity assays (Nan et al. 2008b). Using physiological concentrations of 0.42–1.05 mg/ml pooled heterozygous FH (2.8–7.0 μM), in the absence of phosphate which causes zinc to precipitate, FH was unaffected until [Zn] increased to over 10 μM (Fig. 12a). The use of >10 μM zinc triggered the strong aggregation of FH to form compact oligomers with ill-defined $s_{20,w}$ peaks (Fig. 12b), showing that the FH–zinc K_D value is close to 10 μM. This K_D value means that the bioavailability of only 1% of the several mM zinc observed in drusen is sufficient to cause FH aggregation. Structurally distinct large FH oligomers were also observed for copper. Fluid-phase assays with zinc and copper showed that the reduction of FH activity correlated well with the onset of oligomer formation. It was concluded that the weak binding of zinc to half-sites at the surface of FH caused the cross-linking of the FH monomers to form oligomers (Fig. 13). The implication of weak zinc binding to FH has not always been appreciated. Thus binding studies using radioactive zinc-65 with blotted FH were interpreted to prove that FH did not bind zinc. The weak μM binding of zinc to FH means that any bound radioactive zinc would have been inadvertently removed by washing of the FH blots prior to the radioactivity measurements (Blom et al. 2003).

Further zinc binding studies were performed in order to examine the interaction with homozygous FH (Tyr402 and His402) and its three functionally important recombinant fragments SCR-1/5, SCR-6/8 and SCR-16/20. In order to examine whether FH–zinc oligomers are relevant to AMD, zinc titrations were performed using scattering and ultracentrifugation (Nan et al. 2011). The AMD-risk allotype introduces a His residue which is a potential zinc-binding residue. It turned out that both full-length FH allotypes strongly aggregated again at zinc concentrations above 10 μM (Fig. 12). Despite earlier clues that the His402 allotype might bind more tightly to zinc than Tyr402, no detectable difference between allotypes was seen in the final data analyses. The SCR-6/8 allotypes both aggregated strongly with zinc, indicating that the major zinc binding events occurred there. In comparison to SCR-6/8, the zinc-induced aggregation of SCR-1/5 and SCR-16/20 was lower. Bioinformatics analyses predicted that the SCR-6/8 region had the highest propensity to bind zinc, in support of these experiments. This leads to a schematic view of how zinc-induced FH aggregation occurs to form oligomers (Fig. 13). In conclusion, these interaction studies showed that the zinc inhibition of FH–C3u breakdown in the presence of Factor I is caused by SCR-6/8 aggregation within FH, suggesting that this aggregation sterically blocked the binding of the neighbouring SCR-1/4 domains to C3u.

Conclusions and future considerations

A quantitative understanding of the incompletely formed oligomeric and multivalent complexes formed by FH will permit an understanding of the effect of FH polymorphisms and mutations in causing diseases such as those of AMD and aHUS. For the first time, we have a full set of K_D values for the major FH–ligand complexes (Table 1). The strongest FH interactions are formed by C3b and C3u and these K_D values are with low 1 μM affinities, meaning that FH–C3b and FH–C3u complexes will not be fully formed in plasma. The K_D values for the SCR-1/4 and SCR-19/20 sites are larger and similar (Schmidt et al. 2008). This makes it likely that two molecules of C3b bind separately to FH without synergy between the two sites (Fig. 7a), and there is evidence for this stiochiometry (Li 2010). Ligands such as heparin (an analogue of heparan sulphate on host cells) bind multivalently to FH at two independent sites (Fig. 7c), each with affinities of several μM (Khan 2011). The mechanism by which double-binding of FH to heparin with an overall affinity below 1 μM takes place enables FH to recognise appropriate charge clusters at host cell surfaces. Thus the strength of FH binding to C3b/C3u and to heparin are similar, indicating that FH serves as a scavenger of C3b deposited on host cell surfaces in order to regulate C3b.

The next strongest interactions of FH are with ligands such as C3d (K_D of 3–8 μM and CRP (K_D of 4 μM) (Okemefuna et al. 2009b, 2010b) (Table 1). These weaker affinities concur with the view that, during excess inflammation (acute phase response) with large amounts of C3b present, abundant amounts of C3d and CRP are available. When these are bound to host cell surfaces (Fig. 11), they will provide additional FH binding sites to reinforce host cell protection. Zinc needs to be in large excess in order to inhibit the FH–C3b interaction, given that the FH–zinc K_D is larger still at about 10 μM, however the amount of bioavailable zinc present in drusen (Lengyel et al. 2007) appears sufficient to enable this. The future availability of more K_D values will complete this picture of the FH affinities for its ligands, including a consideration for the effect of other plasma proteins on the FH–ligand interactions.

Many of the discrepancies in the recent FH literature in relation to K_D values result because (i) it is not always appreciated that FH and its C3 and CRP ligands each self-associate (Fig. 4), and that this self-association can be turned to advantage in characterising FH–ligand interactions; (ii) FH interacts weakly with its ligands (Table 1), and consequently the physiologically important FH complexes with its ligands are not fully formed; and (iii) surface plasmon resonance studies to determine K_D values do not give consistent values between different laboratories. If surface plasmon resonance experiments report μM K_D values within the range

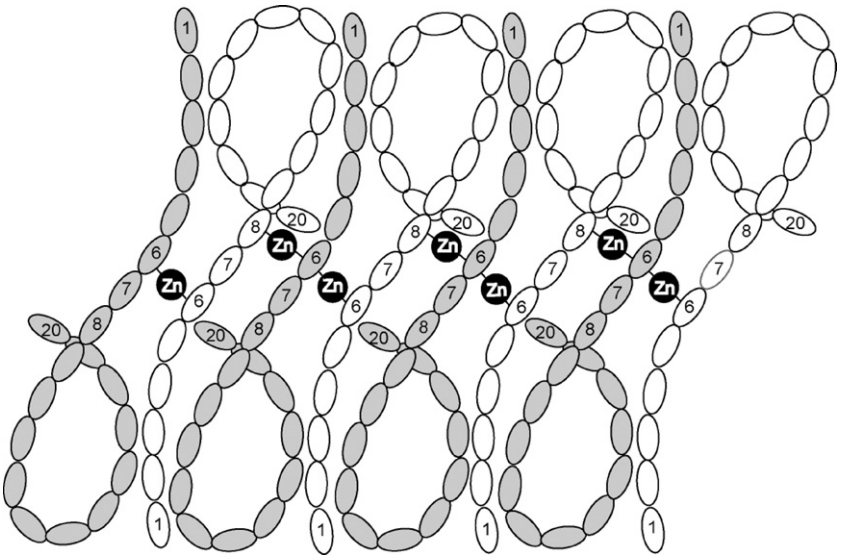

Fig. 13. A schematic model for the FH–zinc interaction. A mechanistic model for the zinc-induced aggregation of FH is based on two possible weak zinc binding sites at the surface of the SCR-6/8 domains. This shows how a daisy-chain of SCR-6/8 domains is formed by sequential zinc sites (Nan et al. 2011). An octamer of FH molecules is shown in alternating white and grey colours. The generalisation of this schematic to all 20 SCR domains in FH explains how FH aggregates and precipitates in the presence of a 100-fold molar excess of zinc.

of a single log unit, the functional conclusions are little affected. From these experiments, if the protein and ligand concentrations are 5 μM while the K_D value is 20 μM, only 17% of the complex will be formed. If the protein and ligand concentrations are 5 μM and the K_D value is 100-fold stronger at 0.2 μM, only 82% of the complex will be formed. The frequent presumption of full 100% complex formation for the FH interactions with C3b, anionic glycosaminoglycan analogues and other ligands in physiological conditions is wrong, even though (for example) it is possible to crystallise FH–C3b complexes. It follows that bacterial evasion strategies that involve the mimicry of FH only require K_D values that are below the μM values for the FH–C3b interaction. It is clear that the most important complement protein–protein interactions with FH correspond to a balance between unbound and bound species. Incomplete complex formation explains the "double-edged sword" of complement activation and regulation (Zipfel and Skerka 2009; Ricklin et al. 2010).

Four different types of FH oligomers have been observed to date:

(i) The oligomers formed through FH self-association are attributed to interactions between pairs of SCR-6/8 and pairs of SCR-16/20 domains. Additional interaction sites are not ruled out. Through self-association, daisy-chains of structurally well-defined FH oligomers are formed that range between dimers and monomers. FH oligomers amount to about 5–14% of the total FH present. Oligomers are formed in a wide range of buffer conditions, implying that FH oligomers exist in not only the test-tube but also in the environment of 70 mg/ml of plasma proteins.
(ii) C3d promotes FH oligomer formation. Using SCR-16/20, as much as 24% of C3d–FH oligomers can be formed in addition to the 5–14% of FH oligomers. The recent crystal structure of SCR-19/20 with two C3d molecules (Kajander et al. 2011) suggests that this results because of two C3d binding sites in SCR-19/20.
(iii) Heparin induces the formation of well-defined ring-like oligomers of FH and heparin in alternation with each other, provided that heparin is dp18 or larger in size. These larger heparin fragments are big enough to crosslink the two heparin sites at SCR-7 and SCR-20 between different FH molecules.
(iv) Zinc induces heavy aggregate formation in FH by cross-linking pairs of half-zinc binding sites within the SCR-6/8 region of FH. Unlike the FH–FH, FH–C3d and FH–heparin oligomers, the FH–zinc aggregates do not possess well-defined structures. Ill-defined FH–copper aggregates are also formed, and these are distinct from those formed by FH–zinc (Nan et al. 2008b).

FH oligomer formation is suppressed by two of the five FH ligands.

(i) The small heparin fragments (dp6, dp12) lead to small decreases in the formation of FH oligomers without cross-linking FH to form large oligomers. This shows that the heparin binding sites compete with those for FH oligomer formation, and was useful in showing that FH and heparin interacted with each other (Khan 2011).
(ii) The addition of CRP to FH suppressed both the formation of FH oligomers and CRP decamers (Fig. 9). This FH–CRP ultra-centrifugation experiment was crucial for establishing that this interaction existed, provided of course that the other complications involving protein concentrations, buffers, and CRP denaturation had been taken into account.

Acknowledgements

We thank University College London, the Medical Research Council, the Biotechnology and Biological Sciences Research Council, the Mercer Fund of the Fight For Sight Charity, the Henry Smith Charity and the Higher Education Commission of Pakistan for studentships and grant funding. We are particularly grateful to Dr Zuby Okemefuna and Dr Daniel Gale at UCL, and Dr Imre Lengyel and Prof Alan Bird of the UCL Institute of Ophthalmology for useful discussions, and Jayesh Gor, Dr Theyencheri Narayanan, Dr Anuj Shukla and Dr Shirley Callow for invaluable instrumental support during our recent projects.

References

Anderson, N.L., 2010. Counting the proteins in plasma. Clin. Chem. 56, 1775–1776.
Aslam, M., Perkins, S.J., 2001. Folded-back solution structure of monomeric Factor H of human complement by synchrotron X-ray and neutron scattering,

analytical ultracentrifugation and constrained molecular modelling. J. Mol. Biol. 309, 1117–1138.
Bhattacharjee, A., Lehtinen, M.J., Kajander, T., Goldman, A., Jokiranta, T.S., 2010. Both domain 19 and domain 20 of factor H are involved in binding to complement C3b and C3d. Mol. Immunol. 47, 1686–1691.
Blom, A.M., Kask, L., Ramesh, B., Hillarp, A., 2003. Effects of zinc on factor I cofactor activity of C4b-binding protein and factor H. Arch. Biochem. Biophys. 418, 108–118.
Christopeit, T., Gossas, T., Danielson, U.H., 2009. Characterization of Ca^{2+} and phosphocholine interactions with C-reactive protein using a surface plasmon resonance biosensor. Anal. Biochem. 391, 39–44.
Clark, S.J., Higman, V.A., Mulloy, B., Perkins, S.J., Lea, S.M., Sim, R.B., Day, A.J., 2006. H384 allotypic variant of factor H associated with age-related macular degeneration has different heparin-binding properties from the non-disease associated form. J. Biol. Chem. 281, 24713–24720.
DiScipio, R.G., 1992. Ultrastructures and interactions of complement factors H and I. J. Immunol. 149, 2592–2599.
Dulbecco, R., Vogt, M., 1954. Plaque formation and isolation of pure lines with poliomyelitis viruses. J. Exp. Med. 99, 167–182.
Fernando, A.N., Furtado, P.B., Clark, S.J., Gilbert, H.E., Day, A.J., Sim, R.B., Perkins, S.J., 2007. Associative and structural properties of the region of complement Factor H encompassing the Tyr402His disease-related polymorphism and its interactions with heparin. J. Mol. Biol. 368, 564–581.
Fenaille, F., Le Mignon, M., Groseil, C., Ramon, C., Riandé, S., Siret, L., Bihoreau, N., 2007. Site-specific N-glycan characterization of human complement factor H. Glycobiology 17, 932–944.
Forneris, F., Ricklin, D., Wu, J., Tzekou, A., Wallace, R.S., Lambris, J.D., Gros, P., 2010. Structures of C3b in complex with factors B and D give insight into complement convertase formation. Science 330, 1816–1820.
Gabay, C., Kushner, I., 2001. Acute-phase Proteins. eLS.
Gilbert, H.E., Eaton, J.T., Hannan, J.P., Holers, V.M., Perkins, S.J., 2005. Solution structure of the complex between CR2 SCR 1-2 and C3d of human complement: an X-ray scattering and sedimentation modelling study. J. Mol. Biol. 346, 859–873.
Good, N.E., Winget, G.D., Winter, W., Connolly, T.N., Izawa, S., Singh, R.M.M., 1966. Hydrogen ion buffers for biological research. Biochemistry 5, 467–477.
Gros, P., Milder, F.J., Janssen, B.J., 2008. Complement driven by conformational changes. Nat. Rev. Immunol. 8, 48–58.
Hakobyan, S., Harris, C.L., Tortajada, A., Goicochea de Jorge, E., García-Layana, A., Fernández-Robredo, P., Rodriguez de Córdoba, S., Morgan, B.P., 2008. Measurement of factor H variants in plasma using variant-specific monoclonal antibodies: application to assessing risk of age-related macular degeneration. Invest. Ophthalmol. Vis. Sci. 49, 1983–1990.
Hellwage, J., Jokiranta, T.S., Friese, M.A., Wolk, T.U., Kampen, E., Zipfel, P.F., Meri, S., 2002. Complement C3b/C3d and cell surface polyanions are recognized by overlapping binding sites on the most carboxyl-terminal domain of complement factor H. J. Immunol. 169, 6935–6944.
Herbert, A.P., Uhrín, D., Lyon, M., Pangburn, M.K., Barlow, P.N., 2006. Disease-associated sequence variations congregate in a polyanion recognition patch on human factor H revealed in three-dimensional structure. J. Biol. Chem. 281, 16512–16520.
Herbert, A.P., Deakin, J.A., Schmidt, C.Q., Blaum, B.S., Egan, C., Ferreira, V.P., Pangburn, M.K., Lyon, M., Uhrin, D., Barlow, P.N., 2007. Structure shows that a glycosaminoglycan and protein recognition site in Factor H is perturbed by age-related macular degeneration-linked single nucleotide polymorphism. J. Biol. Chem. 282, 18960–18968.
Hocking, H.G., Herbert, A.P., Kavanagh, D., Soares, D.C., Ferreira, V.P., Pangburn, M.K., Uhrín, D., Barlow, P.N., 2008. Structure of the N-terminal region of complement factor H and conformational implications of disease-linked sequence variations. J. Biol. Chem. 283, 9475–9487.
Holers, V.M., 2008. The spectrum of complement alternative pathway-mediated diseases. Immunol. Rev. 223, 300–316.
Hurwitz, S., 1996. Homeostatic control of plasma calcium concentration. Crit. Rev. Biochem. Mol. Biol. 31, 41–100.
Janeway, C.A., Travers, P., Walport, M., Schlomchik, M.J., 2005. Immunobiology: The Immune System in Health and Disease. Garland Science Publishing, New York.
Janssen, B.J., Huizinga, E.G., Raaijmakers, H.C., Roos, A., Daha, M.R., Nilsson-Ekdahl, K., Nilsson, B., Gros, P., 2005. Structures of complement component C3 provide insights into the function and evolution of immunity. Nature 437, 505–511.
Jencks, W.P., 1981. On the attribution and additivity of binding energies. Proc. Natl. Acad. Sci. U.S.A. 78, 4046–4050.
Johnson, P.T., Betts, K.E., Radeke, M.J., Hageman, G.S., Anderson, D.H., Johnson, L.V., 2006. Individuals homozygous for the age-related macular degeneration risk-conferring variant of complement factor H have elevated levels of CRP in the choroid. Proc. Natl. Acad. Sci. U.S.A. 103, 17456–17461.
Jokiranta, T.S., Hellwage, J., Koistinen, V., Zipfel, P.F., Meri, S., 2000. Each of the three binding sites of factor H interacts with a distinct site on C3b. J. Biol. Chem. 275, 27657–27662.
Jokiranta, T.S., Jaakola, V.P., Lehtinen, M.J., Parepalo, M., Meri, S., Goldman, A., 2006. Structure of complement factor H carboxyl-terminus reveals molecular basis of atypical haemolytic uremic syndrome. EMBO J. 25, 1784–1794.
Kajander, T., Lehtinen, M.J., Hyvärinen, S., Bhattacharjee, A., Leung, E., Isenman, D.E., Meri, S., Goldman, A., Jokiranta, T.S., 2011. Dual interaction of factor H with C3d and glycosaminoglycans in host-nonhost discrimination by complement. Proc. Natl. Acad. Sci. U.S.A. 108, 2897–2902.
Kinoshita, C.M., Ying, S.C., Hugli, T.E., Potempa, L.A., Jiang, H., Houghten, R.A., Gewurz, H., 1989. Elucidation of a protease sensitive site involved in the binding of calcium to C-reactive protein. Biochemistry 28, 9840–9848.
Khan, S., Gor, J., Mulloy, B., Perkins, S.J., 2010. Semi-rigid solution structures of heparin by constrained X-ray scattering modelling: new insight into heparin–protein complexes. J. Mol. Biol. 395, 504–521.
Khan, S., Rodriguez, E., Patel, R., Gor, J., Mulloy, B., Perkins, S.J., 2011. The solution structure of heparan sulphate differs from that of heparin: implications for function. J. Biol. Chem. 286, 24842–24854.
Khan, S., 2011. Solution structures of glycosaminoglycans and their interactions with complement Factor H. PhD thesis, University College London.
Lengyel, I., Flinn, J.M., Peto, T., Linkous, D.H., Cano, K., Bird, A.C., Lanzirotti, A., Frederickson, C.J., van Kuijk, F.J.G.M., 2007. High concentration of zinc in sub-retinal pigment epithelial deposits. Exp. Eye Res. 84, 772–780.
Li, K., Okemefuna, A.I., Gor, J., Hannan, J.P., Asokan, R., Holers, V.M., Perkins, S.J., 2008. Solution structure of the complex formed between human complement C3d and full length complement receptor Type 2. J. Mol. Biol. 384, 137–150.
Li, K., Gor, J., Perkins, S.J., 2010. Self-association and domain rearrangements between complement C3 and C3u provide insight into the activation mechanism of C3. Biochem. J. 431, 63–72.
Li, K., 2010. Interactions of Complement Receptor Type 2 with C3d and Factor H with C3u. PhD Thesis, University College London.
Lu, J., Stewart, A.J., Sadler, P.J., Pinheiro, T.J., Blindauer, C.A., 2008. Albumin as a zinc carrier: properties of its high-affinity zinc-binding site. Biochem. Soc. Trans. 36, 1317–1321.
Law, S.K.A., Reid, K.B.M., 1995. Complement, second ed. IRL Press, Oxford.
Morgan, H.P., Schmidt, C.Q., Guariento, M., Blaum, B.S., Gillespie, D., Herbert, A.P., Kavanagh, D., Mertens, H.D., Svergun, D.I., Johansson, C.M., Uhrín, D., Barlow, P.N., Hannan, J.P., 2011. Structural basis for engagement by complement factor H of C3b on a self surface. Nat. Struct. Mol. Biol. 18, 463–470.
Nan, R., Gor, J., Perkins, S.J., 2008a. Implications of the progressive self-association of wild-type human Factor H for complement regulation and disease. J. Mol. Biol. 375, 891–900.
Nan, R., Gor, J., Lengyel, I., Perkins, S.J., 2008b. Uncontrolled zinc- and copper-induced oligomerisation of the human complement regulator Factor H and its possible implications for function and disease. J. Mol. Biol. 384, 1341–1352.
Nan, R., Ward, G., Gavigan, L., Miller, A., Gor, J., McKay, A.R., Lengyel, I., Perkins, S.J., 2010. The His402 allotype of complement Factor H show similar self-association to the Tyr402 allotype. Mol. Immunol. 47, 2263 (abstract).
Nan, R., Farabella, I., Schumacher, F., Miller, A., Gor, J., Martin, A.C.R., Jones, D.T., Lengyel, I., Perkins, S.J., 2011. Localisation of the major zinc-binding site of complement Factor H to the SCR-6/8 domains: possible implications for age-related macular degeneration. J. Mol. Biol. 408, 714–735.
Nilsson, B., Ekdahl, K.N., 1998. Components of the alternative pathway. In: Rother, K., Till, G.O., Hansch, G.M. (Eds.), The Complement System. Springer-Verlag, Berlin, pp. 23–49.
Okemefuna, A.I., Gilbert, H.E., Griggs, K.M., Ormsby, R.J., Gordon, D.L., Perkins, S.J., 2008. The regulatory SCR-1/5 and cell-surface-binding SCR-16/20 fragments of Factor H reveal partially folded-back solution structures and different self-associative properties. J. Mol. Biol. 375, 80–101.
Okemefuna, A.I., Nan, R., Gor, J., Perkins, S.J., 2009a. Electrostatic interactions contribute to the folded-back conformation of wild-type human Factor H. J. Mol. Biol. 391, 98–118.
Okemefuna, A.I., Li, K., Nan, R., Ormsby, R.J., Sadlon, T., Gordon, D.L., Perkins, S.J., 2009b. Multimeric interactions between complement Factor H and its C3d ligand provide new insight on complement regulation. J. Mol. Biol. 391, 119–135.
Okemefuna, A.I., Stach, L., Rana, S., Ziai Buetas, A.J., Gor, J., Perkins, S.J., 2010a. C-reactive protein exists in an NaCl concentration dependent pentamer–decamer equilibrium in physiological buffer. J. Biol. Chem. 285, 1041–1052.
Okemefuna, A.I., Nan, R., Miller, A., Gor, J., Perkins, S.J., 2010b. Complement Factor H binds at two independent sites to C-reactive protein in acute-phase concentrations. J. Biol. Chem. 285, 1053–1065.
Oppermann, M., Manuelian, T., Jozsi, M., Brandt, E., Jokiranta, T.S., Heinen, S., Meri, S., Skerka, C., Gotze, O., Zipfel, P.F., 2006. The C-terminus of complement regulator Factor H mediates target recognition: evidence for a compact conformation of the native protein. Clin. Exp. Immunol. 144, 342–352.
Ormsby, R.J., Ranganathan, S., Tong, J.C., Griggs, K.M., Dimasi, D.P., Hewitt, A.W., Burdon, K.P., Craig, J.E., Hoh, J., Gordon, D.L., 2008. Functional and structural implications of the complement factor H Y402H polymorphism associated with age-related macular degeneration. Invest. Ophthalmol. Vis. Sci. 49, 1763–1770.
Pangburn, M.K., Rawal, N., Cortes, C., Alam, M.N., Ferreira, V.P., Atkinson, M.A., 2009. Polyanion-induced self-association of complement factor H. J. Immunol. 182, 1061–1068.
Pepys, M.B., Hirschfield, G.M., 2003. C-reactive protein: a critical update. J. Clin. Invest. 111, 1805–1812.
Perkins, S.J., 1986. Protein volumes and hydration effects: the calculation of partial specific volumes, neutron scattering matchpoints and 280 nm absorption coefficients for proteins and glycoproteins from amino acid sequences. Eur. J. Biochem. 157, 169–180.
Perkins, S.J., Nealis, A.S., Sim, R.B., 1991. Oligomeric domain structure of human complement factor H by X-ray and neutron solution scattering. Biochemistry 30, 2847–2857.
Perkins, S.J., Furtado, P.B., 2005. Complement and immunoglobulin protein structures by X-ray and neutron solution scattering and analytical ultracentrifugation. In: Morikis, D., Lambris, J.D. (Eds.), Structural Biology of the Complement System. Taylor and Francis, Boca Raton, USA, pp. 293–315.

Perkins, S.J., Gilbert, H.E., Lee, Y.C., Sun, Z., Furtado, P.B., 2005. Relating small angle scattering and analytical ultracentrifugation in multidomain proteins. In: Scott, D.J., Harding, S.E., Rowe, A.J. (Eds.), Modern Analytical Ultracentrifugation: Techniques and Methods. Royal Society of Chemistry, London, UK, ISBN 0854045473, pp. 291–319, Chapter 15.

Perkins, S.J., Okemefuna, A.I., Fernando, A.N., Bonner, A., Gilbert, H.E., Furtado, P.B., 2008. Meth. Cell Biol. 84, 375–423.

Perkins, S.J., Okemefuna, A.I., Nan, R., 2010a. Unravelling protein–protein interactions between complement factor H and C-reactive protein by a multidisciplinary strategy. Biochem. Soc. Trans. 38, 894–900.

Perkins, S.J., Nan, R., Okemefuna, A.I., Li, K., Khan, S., Miller, A., 2010b. Multiple interactions of complement factor H with its ligands in solution: a progress report. In: Lambris J.D., Adamis A. (Eds.), Current Topics on Complement and Eye Diseases. Adv. Exp. Med. Biol. 703, 25–47.

Prosser, B.E., Johnson, S., Roversi, P., Herbert, A.P., Blaum, B.S., Tyrrell, J., Jowitt, T.A., Clark, S.J., Tarelli, E., Uhrin, D., Barlow, P.N., Sim, R.B., Day, A.J., Lea, S.M., 2007. Structural basis for complement factor H – linked age-related macular degeneration. J. Exp. Med. 204, 2277–2283.

Putnam, F.W., 1975. The plasma proteins. In: Structure, Function and Genetic Control, second ed. Academic Press, New York.

Ricklin, D., Hajishengallis, G., Yang, K., Lambris, J.D., 2010. Complement: a key system for immune surveillance and homeostasis. Nat. Immunol. 11, 785–797.

Ripoche, J., Day, A.J., Harris, T.J.R., Sim, R.B., 1988. The complete amino acid sequence of human factor H. Biochem. J. 249, 593–602.

Rodriguez de Cordoba, S., Goicoechea de Jorge, E., 2008. Translational mini-review series on complement factor H: genetics and disease associations of human complement factor H. Clin. Exp. Immunol. 151, 1–13.

Rooijakkers, S.H., Wu, J., Ruyken, M., van Domselaar, R., Planken, K.L., Tzekou, A., Ricklin, D., Lambris, J.D., Janssen, B.J., van Strijp, J.A., Gros, P., 2009. Structural and functional implications of the alternative complement pathway C3 convertase stabilized by a staphylococcal inhibitor. Nat. Immunol. 10, 721–727.

Saunders, R.E., Goodship, T.H.J., Zipfel, P.F., Perkins, S.J., 2006. Factor H-associated haemolytic uraemic syndrome: a web database of the structural consequences of disease-associated mutations. Hum. Mutat. 27, 21–30.

Schmidt, C.Q., Herbert, A.P., Kavanagh, D., Gandy, C., Fenton, C.J., Blaum, B.S., Lyon, M., Uhrín, D., Barlow, P.N., 2008. A new map of glycosaminoglycan and C3b binding sites on factor H. J. Immunol. 181, 2610–2619.

Schmidt, C.Q., Herbert, A.P., Mertens, H.D., Guariento, M., Soares, D.C., Uhrin, D., Rowe, A.J., Svergun, D.I., Barlow, P.N., 2010. The central portion of factor H (modules 10–15) is compact and contains a structurally deviant CCP module. J. Mol. Biol. 395, 105–122.

Schmidt, C.Q., Slingsby, F.C., Richards, A., Barlow, P.N., 2011. Production of biologically active complement factor H in therapeutically useful quantities. Protein Expr. Purif. 76, 254–263.

Sharma, A.K., Pangburn, M.K., 1996. Identification of three physically and functionally distinct binding sites for C3b in human complement factor H by deletion mutagenesis. Proc. Natl. Acad. Sci. U.S.A. 93, 10996–11001.

Skerka, C., Lauer, N., Weinberger, A.A., Keilhauer, C.N., Sühnel, J., Smith, R., Schlötzer-Schrehardt, U., Fritsche, L., Heinen, S., Hartmann, A., Weber, B.H., Zipfel, P.F., 2007. Defective complement control of factor H (Y402H) and FHL-1 in age-related macular degeneration. Mol. Immunol. 44, 3398–3406.

Sim, R.B., DiScipio, R.G., 1982. Purification and structural studies on the complement system control protein β_1H (factor H). Biochem. J. 205, 285–293.

Thompson, D., Pepys, M.B., Wood, S.P., 1999. The physiological structure of human C-reactive protein and its complex with phosphocholine. Struct. Fold. Des. 7, 169–177.

Walport, M.J., 2001. Complement. N. Engl. J. Med. 344, 1058–1066, 1140–1144.

Wu, J., Wu, Y.Q., Ricklin, D., Janssen, B.J., Lambris, J.D., Gros, P., 2009. Structure of complement fragment C3b – factor H and implications for host protection by complement regulators. Nat. Immunol. 10, 728–733.

Yu, J., Wiita, P., Kawaguchi, R., Honda, J., Jorgensen, A., Zhang, K., Fischetti, V.A., Sun, H., 2007. Biochemical analysis of a common human polymorphism associated with age-related macular degeneration. Biochemistry 46, 8451–8461.

Zipfel, P.F., Skerka, C., 2009. Complement regulators and inhibitory proteins. Nat. Rev. Immunol. 9, 729–740.